J. Fluid Mech. (1993), *vol.* 256, *pp.* 269–313

A new mechanism for oblique wave resonance in the 'natural' far wake

By C. H. K. WILLIAMSON AND A. PRASAD
Mechanical and Aerospace Engineering, Upson Hall, Cornell University, Ithaca, NY 14853, USA

(Received 21 December 1992 and in revised form 12 May 1993)

There has been some debate recently on whether the far-wake structure downstream of a cylinder is dependent on, or 'connected' with, the precise details of the near-wake structure. Indeed, it has previously been suggested that the far-wake scale and frequency are unconnected with those of the near wake. In the present paper, we demonstrate that both the far-wake scale and frequency are dependent on the near wake. Surprisingly, the characteristic that actually forges a 'connection' between the near and far wakes is the sensitivity to free-stream disturbances. It is these disturbances that are also responsible for the regular three-dimensional patterns that may be visualized. Observations of a regular 'honeycomb'-like three-dimensional pattern in the far wake is found to be caused by an interaction between oblique shedding waves from upstream and large-scale two-dimensional waves, amplified from the free-stream disturbances. The symmetry and spanwise wavelength of Cimbala, Nagib & Roshko's (1988) three-dimensional pattern are precisely consistent with such wave interactions. In the presence of parallel shedding, the lack of a honeycomb pattern shows that such a three-dimensional pattern is clearly dependent on upstream oblique vortex shedding.

With the deductions above as a starting point, we describe a new mechanism for the resonance of oblique waves, as follows. In the case of two-dimensional waves, corresponding to a very small spectral peak in the free stream (f_T) interacting (quadratically) with the oblique shedding waves frequency (f_K), it appears that the most amplified or resonant frequency in the far wake is a combination frequency $f_{FW} = (f_K - f_T)$, which corresponds physically with 'oblique resonance waves' at a large oblique angle. The large scatter in (f_{FW}/f_K) from previous studies is principally caused by the broad response of the far wake to a range of free-stream spectral peaks (f_T). We present clear visualization of the oblique wave phenomenon, coupled with velocity measurements which demonstrate that the secondary oblique wave energy can far exceed the secondary two-dimensional wave energy by up to two orders of magnitude. Further experiments show that, in the absence of an influential free-stream spectral peak, the far wake does not resonate, but instead has a low-amplitude broad spectral response. The present phenomena are due to nonlinear instabilities in the far wake, and are not related to vortex pairing. There would appear to be distinct differences between this oblique wave resonance and the subharmonic resonances that have been previously studied in channel flow, boundary layers, mixing layers and airfoil wakes.

1. Introduction

Although there has been a large number of investigations concerned with the near wake behind a body, there are relatively few papers whose focus has been to study the

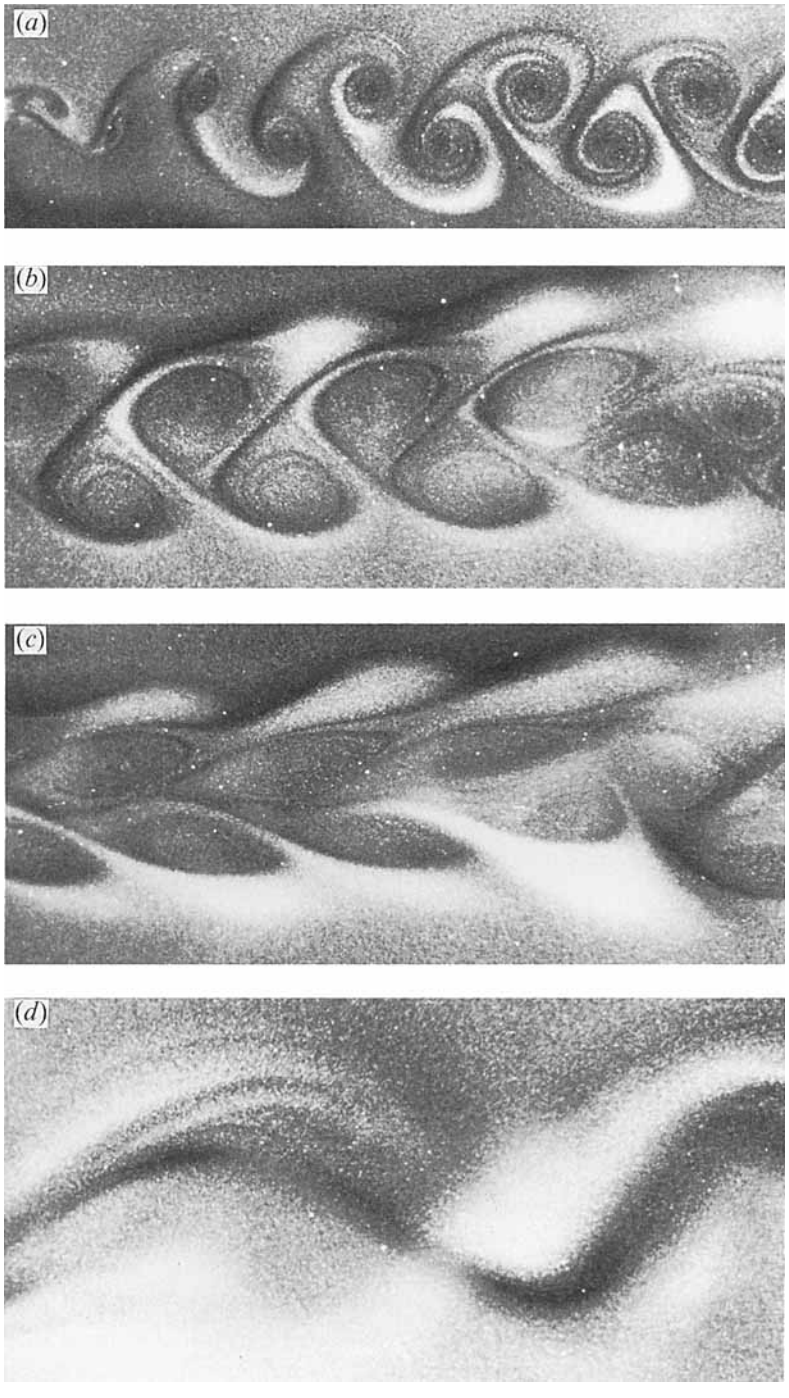

FIGURE 1. The development of a secondary vortex street in the far wake. This visualization sequence of an evolving secondary street was taken from a small water towing tank, in which aluminium flakes were homogenously distributed. A light sheet is used to provide a cross-sectional view of the vortex structures. The flow features may be interpreted as the instantaneous structures (unlike the case with dye or smoke) because the flakes are homogenously distributed and align themselves with the instantaneous stream surfaces. The primary vortex street in (*a*) diffuses as it travels downstream in (*b*) and (*c*). In (*d*), the secondary street is evident, and there is no remaining visual evidence of the primary street.

structure of far wakes. One of the central questions is whether there is a connection between the flow and vortex dynamics right behind a body (in the near wake) and the structure that is found far downstream of a body (in the far wake). In other words, one might question whether the far wake retains a 'signature' of the near-wake dynamics. Of direct relevance to this question is the extent to which background noise (such as in a free stream) influences the development of the far wake, possibly to camouflage the vortical structure that would occur 'naturally'. In the present paper, we address these fundamental questions, by studying in particular the development of the wake behind a nominally two-dimensional body, in this case a long cylinder. This work has been made possible by a recent understanding of three-dimensional effects in the near wake, in particular the influence of end (spanwise) boundary conditions on such flows, and it has been triggered by some simple observations in a wind tunnel.

It has been shown by Roshko (1954) that there exist three regimes of flow at low to moderate Reynolds numbers (*Re*), namely the laminar, transition and irregular (turbulent) regimes, each of which occurs within certain ranges of *Re*. The transition regime is associated with the inception of small-scale structure (Hama 1959; Gerrard 1978). Recent studies by Williamson (1988*b*, 1991, 1992*a*) show that the transition regime (roughly $Re = 180$–260) involves not only small-scale streamwise vortex structures and vortex loops, but also massive spot-like structures caused by 'vortex dislocations' and which form when there is a phase discontinuity in the vortex shedding. However, three-dimensionality is also a central feature of the laminar regime at lower Reynolds numbers in both the near wake and far wake. Loosely defined, the near wake extends for a few diameters downstream of the body in the region where the vortices roll up and shed, whereas the far wake defines a region where the velocity fluctuations are small, and extends up to several hundreds of diameters downstream. In both the laminar and turbulent wake regimes, the width of a nominally two-dimensional far wake grows as $x^{\frac{1}{2}}$, for large values of downstream distance (x), and we thus expect the size of the far-wake structures to increase, while the passage frequency of these structures should decrease.

Some original observations by Taneda (1959) demonstrated the decay of the original Kármán street wake and the growth in the far wake of a secondary vortex-street structure of larger scale and lower frequency. The development of such a secondary vortex street is shown in figure 1, taken from a small towing tank (by the first author at Caltech in 1985) in which aluminium flakes were homogenously distributed within the fluid. The primary vortex street in (*a*) diffuses as it travels downstream in (*b*) and (*c*). In (*d*), the secondary street is evident, and there is no remaining visual evidence of the primary street. Taneda suggested that such a far-wake periodic structure (which scales approximately on the local wake width) arises out of a hydrodynamic instability based on the local mean velocity profile. The ratios for the wavelength of downstream structure to upstream structure were found to range from 1.8 to 3.6. In contrast to this view of hydrodynamic instability, a different interpretation of the growth of the far wake was then put forward by Matsui & Okude (1981, 1983). They suggested that the secondary street is generated by vortex amalgamations or pairing of the original Kármán vortices into larger vortical structures. Support for this argument comes from flow visualizations which show blobs of smoke formed by the upstream individual vortices pairing up further downstream, although it was stated that not all of the vortices paired up with each other. The above two interpretations for the growth of the far-wake secondary structure were later summarized by Cimbala, Nagib & Roshko (1988) as follows:

(*a*) *Hydrodynamic instability of the local mean velocity profile in the far wake.* This instability mechanism is responsible for the growth of a secondary structure, and is

independent of the vortices shed from the body. The secondary street does not directly result from vortex amalgamations (pairing), although vortex pairing might occur incidentally.

(*b*) *Discrete vortex interactions* (*vortex pairing*). In this mechanism it is supposed that the secondary large-scale street is formed by amalgamation of primary Kármán street vortices into larger vortical structures.

Support for the pairing or vortex amalgamation mechanism might be inferred from other shear flows, for example the mixing layer, where the work of Brown & Roshko (1974) and Winant & Browand (1974) demonstrated that pairing and discrete vortex amalgamations is an essential aspect of shear-layer growth. It may also be shown from stability analysis of point vortex configurations that a single row of vortices (Lamb 1932) as well as an infinite vortex street configuration (Saffman & Schatzman 1982) is most unstable to a pairing instability. A more recent study by Meiburg (1987) suggests, from numerical computation of fundamental and subharmonic perturbations imposed on two vorticity layers, that vortex pairing is able to account for the growth of a secondary vortex street. He also showed that, without a fixed phase relation between the subharmonics developing in each vorticity layer, one may not necessarily expect the pairing process to be reflected by a spectral peak precisely at $\frac{1}{2}f_K$ (where f_K is the Kármán shedding frequency) although peaks close to this value would occur, which is consistent with the experiments of Cimbala (1984).

An incisive experimental study by Cimbala (1984), and by Cimbala, Nagib & Roshko (1981, 1988) suggested that the far-wake structure does not depend directly on the scale or frequency of Kármán vortices shed from the cylinder, and correspondingly that the growth of the secondary structure is due to hydrodynamic instability of the developing mean wake profile. The facts that frequencies unrelated to the Kármán shedding frequency (f_K) were amplified in the far wake, and that they were close to those frequencies predicted from stability analysis, strongly suggest that hydrodynamic instability is the principal mechanism for secondary street growth. It should be noted that it is difficult to choose a particular single frequency to represent the far wake, since a broad band of frequencies are selectively amplified and then damped, and the centre of the band shifts to lower frequencies, as the flow travels downstream.

Further related studies by Desruelle (1983) and by Cimbala & Krein (1990) demonstrate the strong sensitivity of the far wake to external noise. Desruelle acoustically forced the wake using a speaker and, of direct relevance to the present work, he found that often the principal response occurred at the combination frequency ($f_K - f_T$) rather than at the imposed frequency (f_T) itself. A similar response of combination frequencies was found by Cimbala & Krein when they deliberately interfered with the spectral peaks in the free-stream spectrum. The significant receptivity of the far wake to the intricacies of the low-turbulence free-stream spectrum is consistent with the far-wake growth being due to hydrodynamic instability.

A further major contribution from the work of Cimbala (1984) and Cimbala *et al.* (1988) comes from planview (spanwise) flow visualization, which showed, for the first time, a 'honeycomb-like' cellular three-dimensional pattern in the far wake (see our figure 4). They suggested that this cellular three-dimensional pattern could be caused by a secondary three-dimensional parametric instability of the subharmonic type acting on the far-wake initially two-dimensional waves, in analogy with subharmonic resonances found in mixing layers (Pierrehumbert & Widnall 1982) and in boundary layers (Herbert 1988). With regard to this honeycomb pattern, it was later stated by Coles (1985) that further study of this phenomenon in the wake should be classified as 'urgent unfinished business', particularly since it has relevance to three-dimensional

structure in other shear flows. An explanation of this phenomenon is a central part of the present work.

Investigations which involve forcing three-dimensional structure in far wakes have been undertaken by Lasheras & Meiburg (1990) and by Corke, Krull & Ghassemi (1992). Lasheras & Meiburg carried out a combined numerical–experimental study on an unseparated wake, where they induced both two-dimensional waves and also pairs of (equal and opposite) subharmonic oblique waves in the computations. The evolving three-dimensional structures (in planview) show a marked similarity with the pictures of Cimbala *et al.* Corke *et al.* (1992) have also forced two-dimensional waves simultaneously with three-dimensional subharmonic oblique wave pairs in the unseparated wake from a symmetric airfoil (using a mosaic of computer-controlled piezoelectric transducers), and found that indeed a parametric resonance can exist. (This work is related to the original 'triad' resonance in boundary layers introduced by Craik (1971) and which, in that case, required the two-dimensional and three-dimensional subharmonic waves to be eigensolutions of the Orr–Sommerfeld equations.) In agreement with the analysis of Flemming for the same perturbed flow, they showed that there exists a threshold amplitude for the two-dimensional waves above which the subharmonic three-dimensional resonance will occur. Similar studies by Corke (1993), with oblique wave pairs that are *not* the subharmonic of the two-dimensional wave, show that 'generations' of combination frequencies are amplified as the flow travels downstream.

A new understanding of some *near-wake* three-dimensionalities is now altering our interpretations of *far-wake* phenomena. In the near wake, it has recently been shown that oblique shedding (where vortices are shed at some angle to the cylinder axis) is caused by influences from the end boundary conditions, for cylinders of even hundreds of diameters in length, but that with suitable manipulation of the end conditions, parallel (two-dimensional) shedding may be induced (Williamson, 1988*a*, 1989*a*; Eisenlohr & Eckelmann 1989; Koenig, Eisenlohr & Eckelmann 1990; Hammache & Gharib 1989, 1991). Of significance to the present study is the fact that the shedding frequency is reduced as the oblique angle of shedding (θ) is increased. It was suggested in Williamson (1991) that there is a direct link between the near-wake phenomenon of oblique shedding and the far-wake honeycomb pattern of Cimbala *et al.* (1988). It was observed that, if there is oblique shedding, then the downstream structure involves the evolution of what appeared to be oblique instability waves at an angle typically around twice the original oblique shedding angle, and with the same orientation. It was suggested that the origin of the oblique disturbances in the far wake is an interaction between the oblique shedding from upstream with two-dimensional waves from downstream. These simple conclusions are confirmed by the present investigation.

The present work was triggered at Cornell from an undergraduate research project in 1990 undertaken by Kristen Gledhill, who set up a new smoke wire visualization system in our wind tunnel. By viewing a cylinder wake in planview, we immediately demonstrated inadvertently but rather clearly the three-dimensional honeycomb patterns discussed above. It was clear that in our facility the pattern was the direct result of an interaction between oblique shedding vortices and parallel (two-dimensional) large-scale waves which grew in the far wake. With parallel shedding upstream, we found no honeycomb pattern downstream. These preliminary results were presented by Williamson at the ONR Wakes Workshops in 1991, 1992 and in Williamson (1992*b*). It was also shown that the pattern originally observed by Cimbala *et al.* (1988) is indeed the same phenomenon. Simple geometrical relationships for the relevant angles and wavelengths for the interacting wave pattern show that the

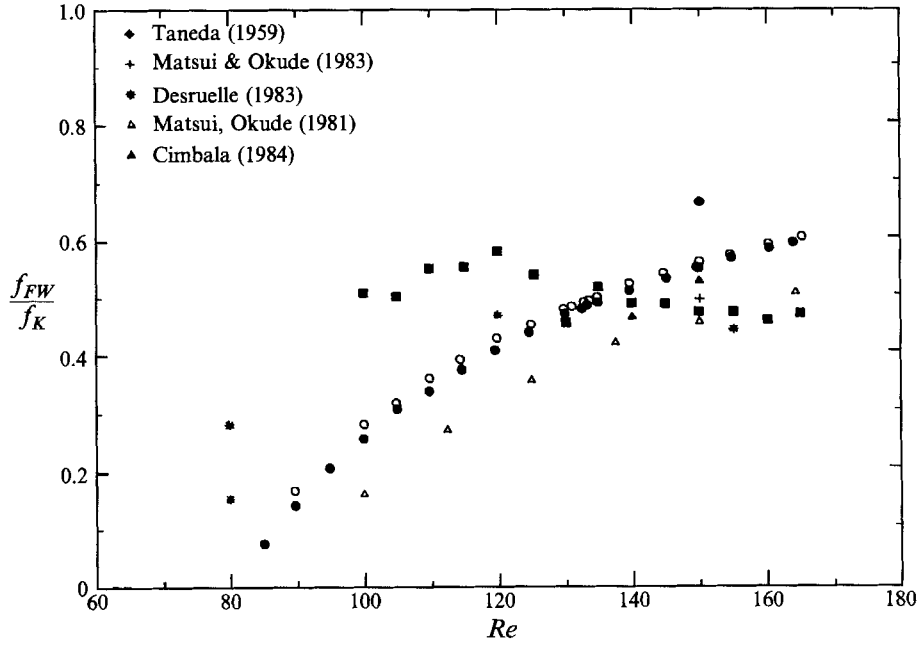

FIGURE 2. Measurements of far-wake frequency, showing the large scatter amongst measurements of (f_{FW}/f_K) versus Re found in the literature. The circles and squares are present data (evaluated at $x/D = 150$).

spanwise wavelength of the honeycomb pattern is equal to the spanwise wavelength of the oblique shedding vortices, and that the geometry of the honeycomb pattern is obviously influenced by the angle of oblique shedding. These simple results, which appear in Williamson & Prasad (1993*a*), form the starting point for the present investigation.

It should be mentioned that important results of Hammache & Gharib pertaining to the far wake were also presented at the above Workshops and in Hammache (1991), and Hammache & Gharib (1992). In agreement with the conclusions of Cimbala *et al.* (1988), they state that no direct relationship should be expected between the frequencies in the primary and secondary regions. Indeed, they find that, past the region of decay of the Kármán street, the secondary vortices are parallel (two-dimensional) irrespective of whether there is oblique shedding or parallel shedding upstream and, correspondingly, the far-wake frequency is found to be independent of the Kármán frequency. If there is oblique shedding upstream, a spanwise waviness exists on the parallel far-wake waves. Some careful measurements at different spanwise locations demonstrate clearly that the spanwise wavelength of the downstream pattern is equal to the spanwise wavelength of the oblique shedding vortices. This constitutes a 'connection' between the near and far wake. Both of these conclusions are in complete agreement with our own work.

We present here in figure 2 a compilation of previous and present data for the ratio of far-wake frequency to near-wake frequency (f_{FW}/f_K), over a range of Re. It can be seen that there exists a great deal of scatter. Although some of this scatter may be caused by differences in oblique shedding angle (and thereby frequency f_K) as suggested by Hammache & Gharib, the wide disparities may be due also to other effects. This is one of a number of questions that are addressed in the present work. A central question

is whether the far wake can, in fact, be connected to the near-wake structure *both in scale and frequency*. Secondly, it is of interest to investigate further the two mechanisms for secondary wake growth, namely hydrodynamic instability or vortex amalgamation. Thirdly, there is the question of the origin of the honeycomb-like three-dimensional pattern of Cimbala *et al.* in the far wake. Although it is reasonably clear from simple observation of their visualization that such a pattern is caused by parallel and oblique waves interacting, one might ask from where these waves originate? Finally, a further significant question can be posed: Are the combination frequencies discussed earlier indicative of some physical structure (i.e. waves)? It will be seen that the answer to this final question is at the heart of this paper.

In §3, we shall demonstrate that the honeycomb three-dimensional pattern in the far wake is caused by an interaction between two wave systems: the oblique shedding waves from upstream and the parallel (two-dimensional) large-scale waves which become amplified in the far wake. Measurements of frequency in §4 show that, in our flow, there is a combination-frequency response in the far wake equal to $(f_K - f_T)$, where (f_K) is the Kármán frequency and (f_T) is a constant frequency associated with the free-stream noise. Thus the far-wake frequency as well as the scale are 'connected' to the near wake. It is shown in §5 that the frequency (f_T) corresponds to parallel (two-dimensional) waves in the far wake. A significant result is that the combination frequency $(f_K - f_T)$ corresponds to an 'oblique resonance wave' of large angle. The initial interaction of two waves of small amplitude leads to the resonance of a third one, whose amplitude may exceed the first two by an order of magnitude. In §7, we show that two modes of oblique wave resonance can exist, depending on whether (f_T/f_K) is greater or less than $\frac{1}{2}$. Experiments with a smaller cylinder in §8 enable us to investigate the far wake under conditions of very low free-stream noise, where no resonances are found. In §9, we show, using Cimbala *et al.*'s (1988) stability calculations, that the oblique wave resonance occurs when the oblique waves curve in the (f, Re)-plane falls within the unstable region defined by the neutral stability curve. We study the cause of the small spectral peak (f_T) in the free stream in §10, followed by discussion and conclusions.

2. Experimental details

Measurements of velocity fluctuations were made with a miniature hot wire situated in the wake of a cylinder of diameter 0.001 08 m, in a 0.305 m square test section (12 in. × 12 in.) of an open-circuit suction wind tunnel. The turbulence level was close to 0.08 %, with flow uniformity better than 0.3 %. A good deal of effort was taken to isolate the cylinder from the tunnel, and to damp out any cylinder vibrations. Flow visualization was conducted using a smoke wire system, in the manner originally described by Corke *et al.* (1977).

The origin of the wake coordinate system is fixed on the axis of the cylinder. The x-axis is downstream, the y-axis is perpendicular (defined as transverse) to the flow direction and to the cylinder axis, and the z-axis lies along the axis of the cylinder (defined as spanwise).

3. Origin of the honeycomb-like three-dimensional pattern in the far wake

The present investigation was triggered principally by some smoke-wire visualizations shown in figure 3. In this case, a smoke wire is placed upstream of the cylinder (vertical line at the extreme left) and the oblique shedding vortices are shown as the set of white lines at some oblique angle to the vertical cylinder. At a certain point

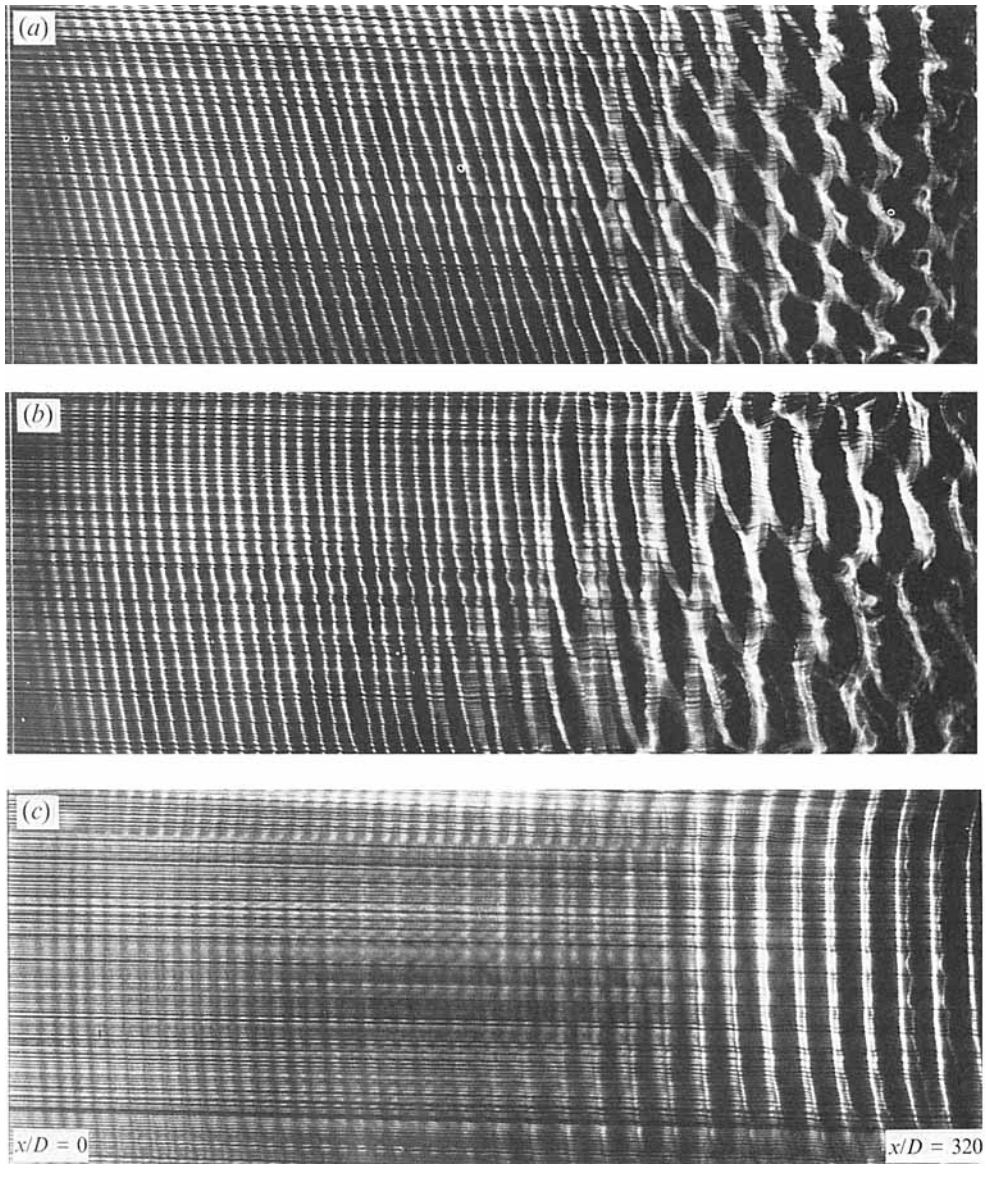

FIGURE 3. Demonstration of a direct link between the honeycomb-like pattern and the existence of oblique vortex shedding. The far-wake honeycomb pattern is caused by the interaction of oblique shedding waves with large-scale parallel (two-dimensional) waves in the far wake. The angle of oblique shedding influences the structure of the honeycomb pattern as shown in (*a*) and (*b*), most obviously the spanwise wavelength, which is precisely equal to the spanwise wavelength of the oblique vortices. If there is parallel shedding in (*c*), then there is no honeycomb pattern in the far wake.

downstream (the flow travels to the right), it can be seen clearly that the oblique vortices become deformed by two-dimensional waves to yield a honeycomb-like pattern in the far wake. From (*a*) and (*b*) it can be seen that the geometry of the honeycomb pattern is obviously influenced by the oblique shedding angle. It is straightforward to demonstrate, from the geometry of the intersecting wave pattern,

that the spanwise wavelength of the honeycomb pattern λ_{ZH} is equal to the spanwise wavelength of the oblique shedding vortices, λ_{ZK}:

$$\lambda_{ZH} = \lambda_{ZK} = \lambda_K / \tan\theta_K, \tag{1}$$

where λ_K is the streamwise wavelength of the oblique shedding vortices and θ_K is the oblique shedding angle. Therefore as the shedding angle (θ_K) is reduced in (*b*), relative to (*a*), so the honeycomb spanwise wavelength (λ_{ZH}) increases. Of particular significance is the fact that, in the presence of parallel shedding in (*c*), the evident lack of a honeycomb three-dimensional pattern shows that the pattern here is clearly dependent on the oblique vortex shedding.

A natural question at this point is whether the honeycomb pattern of Cimbala *et al.* (1988) is caused by the same wave interactions. In order to address this question, we show, in figure 4, the three-dimensional pattern observed by Cimbala *et al.* (from their figure 19*c*) in the lower photograph in (*b*), as well as our own visualization above in (*a*). In the top photograph, if we draw a white line through the honeycomb pattern at the oblique shedding angle of 22°, it clearly passes through a line of symmetry of the honeycomb pattern, a result which is not unexpected. We similarly draw a white line through the honeycomb pattern of Cimbala *et al.* in the photograph below, in this case at their oblique shedding angle (measured as 14° from their corresponding figure 19*a*). Again, we find that it represents the same line of symmetry in their three-dimensional pattern as it does in our visualization. A further measurement of spanwise wavelength for their honeycomb pattern gives $(\lambda_{ZH}/\lambda_K) = 4.1$, while a measurement of spanwise wavelength for their oblique shedding vortices (their figure 19*a*) yields $(\lambda_{ZH}/\lambda_K) = \tan^{-1}(14°) = 4.0$, which shows that $\lambda_{ZH} = \lambda_{ZK}$, to the accuracy of measurement. There would seem little question, from the above evidence, that the honeycomb pattern of Cimbala *et al.* is caused by the same wave interaction phenomenon as found in the present study, namely their oblique shedding waves interacting with growing two-dimensional waves in the far wake.

It would appear that these results show, in a most straightforward manner, that the far-wake honeycomb pattern is triggered by a hydrodynamic instability of large-scale parallel (two-dimensional) waves, rather than by vortex pairing, in agreement with the already extensive evidence presented in Cimbala *et al.* The basis of this statement lies in the fact that the evolving large-scale waves of the far wake are two-dimensional, while the shedding vortices are oblique. If vortex pairing were the main mechanism for far-wake growth, then one would expect the oblique vortices to pair along their length at an oblique angle, which has not been observed in the far wake. However, this does not preclude the far-wake frequency being (coincidentally) a subharmonic of the near-wake frequency.

Although it was hitherto believed that there was no direct connection between near and far wakes, the straightforward observations shown here demonstrate that the near and far wakes are indeed directly connected. It will be demonstrated in the following section that the far-wake frequencies can also be directly influenced by the near-wake Kármán frequency.

4. Measurements of frequency in the far wake

Measurements of frequency in the far wake (f_{FW}) over a range of Reynolds number, presented in figure 5 (*a*), show that the predominant peak in the spectrum, in our experiments, corresponds to a combination frequency:

$$f_{FW} = f_K - f_T, \tag{2}$$

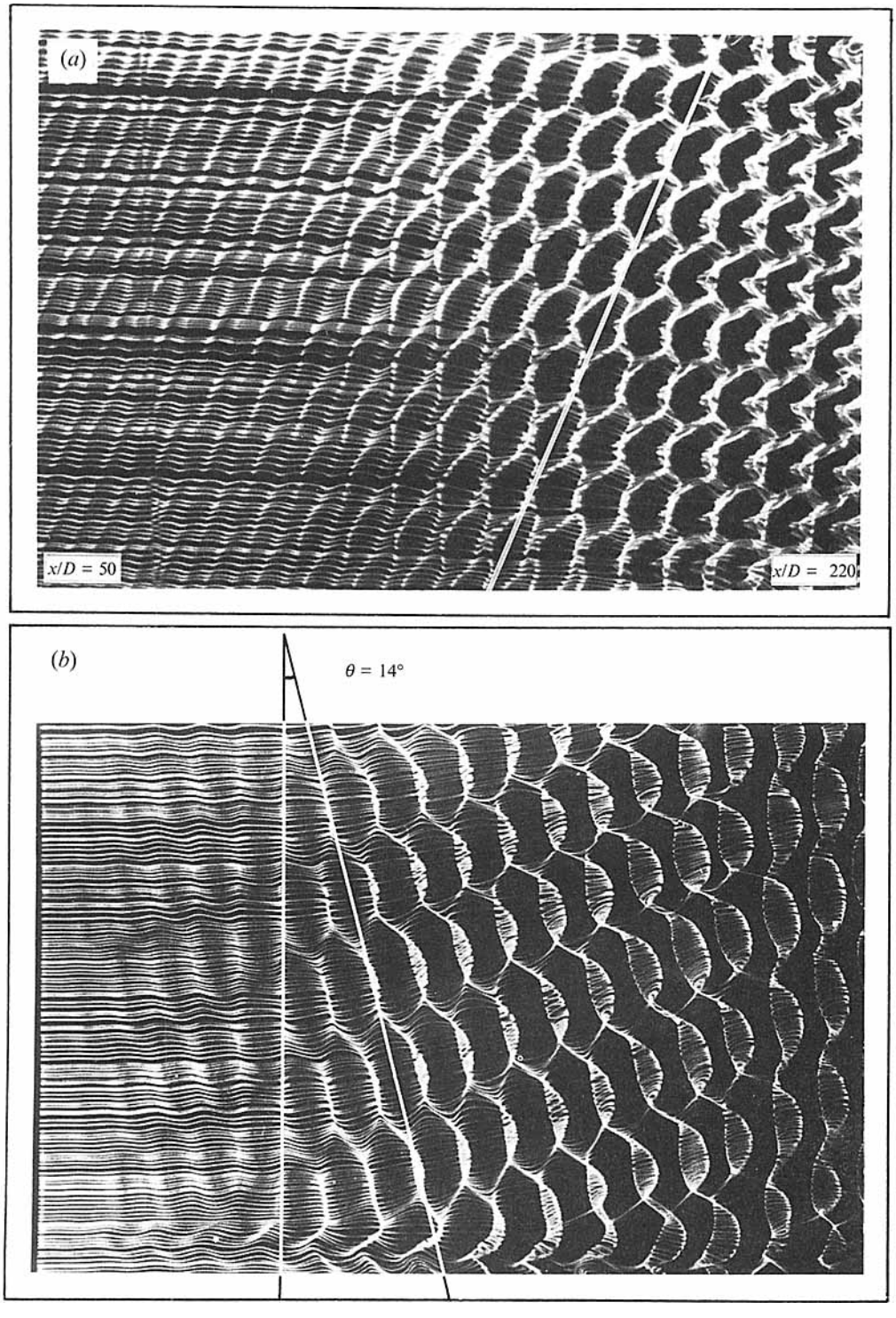

FIGURE 4. Demonstration that the honeycomb pattern of Cimbala *et al.* (1988) is caused by oblique shedding waves interacting with far-wake two-dimensional waves. Oblique vortices may be seen in (*a*) (our visualization) being deformed by two-dimensional waves in the far wake, as they travel to the right. The oblique shedding angle is drawn as the white line in the honeycomb pattern, and it can be

where f_K is the Kármán frequency upstream, and f_T represents a surprisingly small peak that we have found to be associated with the free stream in our tunnel. (We shall show later that $(u'_{rms}/U) = 0.00005$ for the frequency f_T.) In other words, the far-wake frequency has a constant difference of f_T (= 159 Hz) from the shedding frequency, as shown in (*a*). This phenomenon is in accordance with the results of Cimbala & Krein (1990), who demonstrated an extreme sensitivity of the far wake to even very small disturbances in the free stream. In their case, the far wake was rather more complicated, owing to the presence of a whole group of small peaks in the free-stream spectrum.

Since the far-wake frequency corresponds to $f_{FW} = (f_K - f_T)$, one can see that changes in the upstream shedding frequency f_K, at a given Reynolds number, will alter f_{FW}. This means that the far-wake frequency is affected by whether there is parallel or oblique shedding upstream, since f_K is a function of oblique shedding angle. The frequency measurements in figure 5(*b*) show that indeed this is the case, and from (2) the differences in far-wake frequency for oblique or parallel shedding are equal to the differences in upstream frequency. We can make an estimate of the differences in the ratio (f_{FW}/f_K) that can be attributed to whether the shedding is parallel or oblique, as follows:

$$\Delta(f_{FW}/f_K) = (f_0 - f_\theta)/f_0 = 1 - \cos\theta, \tag{3}$$

where (f_0) is the parallel shedding frequency, (f_θ) is the oblique shedding frequency, and θ is the oblique shedding angle. In this expression, we have made use of the $\cos\theta$ transformation relating f_0 and f_θ found in Williamson (1988*a*, 1989*a*). For typical oblique angles of around $\theta = 15°$, the ratio (f_{FW}/f_K) will vary by up to 4% depending on whether the shedding angle is parallel or oblique. We see in figure 2 that the scatter in previously measured values for (f_{FW}/f_K) can be of the order of 50%, so that variations in oblique shedding angle alone cannot explain the discrepancies.

It appears that it is the extreme sensitivity of the far wake to the free-stream spectral peaks that causes the large scatter in previous measurements of (f_{FW}/f_K). If there are small free-stream peaks at various values of normalized (f_T/f_K) in other facilities, then combination (or possibly direct) response frequencies in the far wake given by

$$f_{FW}/f_K = 1 - f_T/f_K \tag{4}$$

would cause a significant variation, sufficient to explain the large scatter in the literature in figure 2. We shall demonstrate a broad receptivity to different values of (f_T/f_K) in Williamson & Prasad (1993*b*), and also show in §11 that the data of Matsui & Okude (1983) correspond to a combination-frequency response of the far wake.

A significant fundamental question remains at this point: Does the existence of a combination frequency reflect the presence of any physical structure in the flow (i.e. waves)? This question is addressed directly in the following section.

5. Oblique wave resonance in the far wake

In the flow visualization shown earlier, one can observe large-scale parallel (two-dimensional) waves in the far wake, whereas the predominant frequency in the far wake (as measured above) is the combination frequency $(f_K - f_T)$. We initially assumed that these two-dimensional waves corresponded with that combination frequency.

---

seen that it represents a line of symmetry in this pattern. The honeycomb pattern observed by Cimbala *et al.* (1988) shown in (*b*) demonstrates that their oblique shedding angle (14°) represents the same line of symmetry in their pattern.

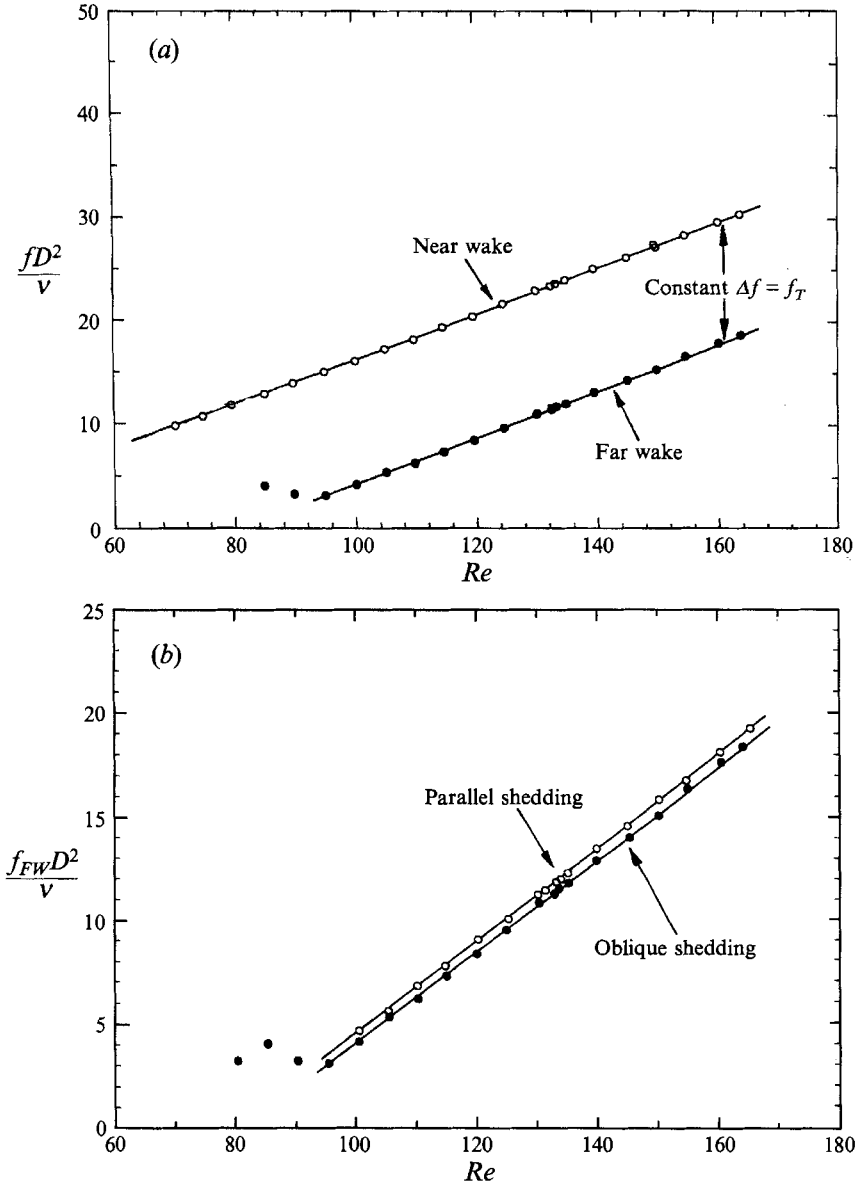

FIGURE 5. Measurement of normalized far-wake frequency versus *Re*. In (*a*), we show that there is a constant frequency difference (f_T) between the near-wake frequency (f_K) and the far-wake frequency (f_{FW}). This demonstrates the response of the far wake to a combination frequency $f_{FW} = (f_K - f_T)$. In (*b*), we show the small differences in far-wake frequency caused by whether the shedding upstream is parallel or oblique.

However, further visualization showed that the wavelength of the two-dimensional waves increases with Reynolds number, as shown in the photographs of figure 6. By visually measuring these wavelengths (λ), we were further able to show that the wavelength of these parallel waves is proportional to Reynolds number, as seen in the

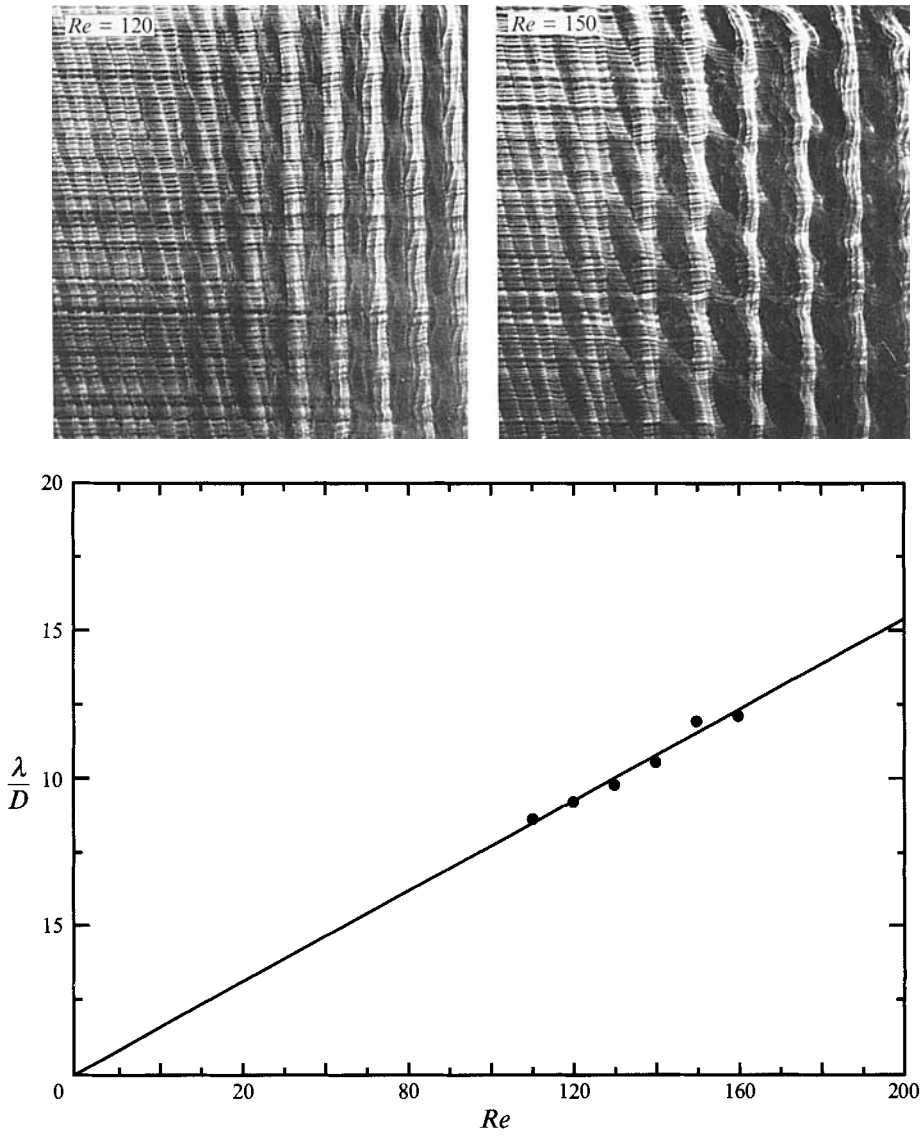

FIGURE 6. Observations and measurements of wavelength for two-dimensional waves in the far wake, versus *Re*. The linear relationship between the normalized wavelength (λ/D) and Reynolds number (*Re*) is demonstrated.

plot of figure 6. It is then reasonable to conclude that the parallel waves correspond to a constant frequency. It can be shown that

$$\frac{\lambda}{D} = \frac{U_W/U_\infty}{f_T D^2/\nu} Re = (\text{gradient of plot}) \times Re, \tag{5}$$

where U_W is the phase speed of the waves, U_∞ is the free-stream velocity, D is the cylinder diameter, and ν is the kinematic viscosity. If we assume for the moment that the constant frequency in the above expression is indeed $f_T = 159$ Hz, then using the

value for the least-squares gradient of the plot, we find that the normalized phase speed for the waves becomes $(U_W/U_\infty) = 0.93$. This is consistent with the phase velocity $(U_W/U_\infty) = 0.92$ for two-dimensional (parallel) waves found in the far wake of a symmetric airfoil by Corke *et al.* (1992). It appears from the above that the parallel waves are indeed associated with the frequency f_T. Following this conclusion, one might question what should be seen in visualizations that would correspond to the combination frequency $(f_K - f_T)$.

It seems established from analytical investigations of boundary layers and other flows (for example Raetz 1959, Stuart 1962 and Craik 1985) that the nonlinear interaction of two waves can lead to other waves at sum and difference (combination) frequencies that can, under some circumstances, become amplified to comparable or greater amplitudes than the original waves, in a form of resonance. For such resonance, it is required that the two waves travel at the same phase speed (i.e. become phase-locked). Let us consider the following two waves:

$$a_1 e^{i(\alpha_1 x + \beta_1 z - \omega_1 t)}, \tag{6}$$

$$a_2 e^{i(\alpha_2 x + \beta_2 z - \omega_2 t)} \tag{7}$$

With such a two-wave interaction, one may expect quadratic terms of order (a^2) to appear, i.e. terms formed by products of the above waves and their complex conjugates (but not necessarily to resonate), for example, $(a_1 a_2)$, $(a_1 a_2^*)$, etc. The second of these nonlinear terms, involving the difference frequency $(\omega_1 - \omega_2)$, would directly relate to the present problem. Let us denote this third wave corresponding to $(a_1 a_2^*)$ as

$$a_3 e^{i(\alpha_3 x + \beta_3 z - \omega_3 t)}, \tag{8}$$

where the following relationship may be written:

$$\omega_3 = \omega_1 - \omega_2, \tag{9}$$

$$\beta_3 = \beta_1 - \beta_2, \tag{10}$$

$$\alpha_3 = \alpha_1 - \alpha_2. \tag{11}$$

A resonance exists if such a relationship between three waves holds true, and this is what is present in our flow. For our system of waves, subscript 1 refers to the Kármán oblique shedding waves, which we shall henceforth denote with subscript K. The other wave system with subscript 2 refers to the large-scale two-dimensional waves, now denoted with subscript T. The two interaction waves $(a_1^* a_2)$ and $(a_1^* a_2^*)$ correspond to negative frequencies in our problem, and the wave $(a_1 a_2)$ corresponds to a frequency $(f_K + f_T)$, which would be linearly damped even more than the decaying Kármán waves. This leaves us with only $(a_1 a_2^*)$. If the difference frequency is denoted $f_{\theta 1}$, then (9) becomes

$$f_{\theta 1} = (f_K - f_T). \tag{12}$$

We can then look to the other two relations for the geometry of the wave corresponding to this frequency. If the spanwise wavelength of the combination wave is written as $\lambda_{Z\theta}$ and the spanwise wavelength for the oblique shedding wave as λ_{ZK}, (10) gives (with $\beta_T = 0$)

$$\lambda_{Z\theta} = \lambda_{ZK}, \tag{13}$$

which can, in any case, be seen immediately from the geometry, and was discussed for the honeycomb pattern in the Introduction. Referring now to the streamwise wavelength of the combination wave as $\lambda_{\theta 1}$, (11) gives

$$\frac{\lambda_{\theta 1}}{\lambda_K} = \frac{\lambda_T/\lambda_K}{\lambda_T/\lambda_K - 1}. \tag{14}$$

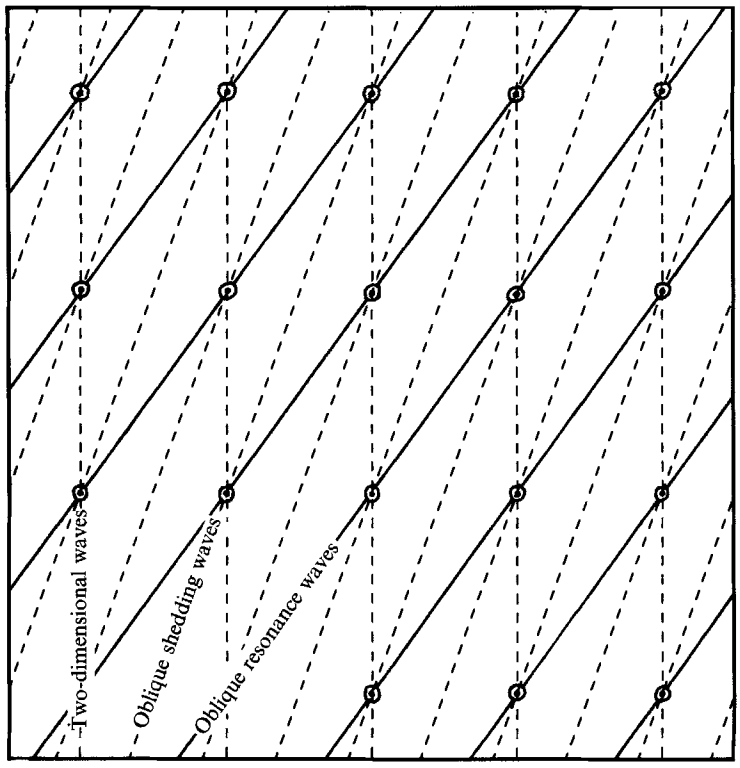

FIGURE 7. Diagram showing that oblique resonance waves join nodes formed by the interaction of oblique shedding waves and two-dimensional waves.

The angle of the combination wave θ_1 (angle measured relative to the two-dimensional wave) can be found, using (13), as

$$\frac{\tan\theta_1}{\tan\theta_K} = \frac{\lambda_{\theta 1}}{\lambda_K}. \tag{15}$$

Before connecting the above ideas with possible observation of waves at the combination frequency, we shall discuss how different waves might be formed in this wake flow. As the primary oblique shedding vortices (waves) travel downstream (to the right in figures 3 and 4) so they become deformed by the large-scale parallel waves. As this deformation grows, parts of the oblique shedding waves align themselves along a line of symmetry in the pattern to form a new set of large-scale large-angle oblique waves. This picture of the deformations assumes that the original oblique lines remaining in the far wake correspond to some residual non-negligable fluctuations of the oblique shedding waves (which is supported by our later spectral measurements and by data of Matsui & Okude 1983).

From the geometry of this problem given by the equations above, and shown in figure 7, we can see that these large-angle oblique waves correspond simply to the lines joining the nodes of the intersection pattern formed by the original two sets of waves. If these combination waves at frequency $f_{\theta 1} = (f_K - f_T)$ are the most amplified waves in the far wake (in preference to the parallel waves at least over some downstream region), then we should expect the frequency $f_{\theta 1}$ to correspond to an 'oblique wave resonance' which should be observed in flow visualization.

In the experiment, the observation of such oblique resonance waves initially proved

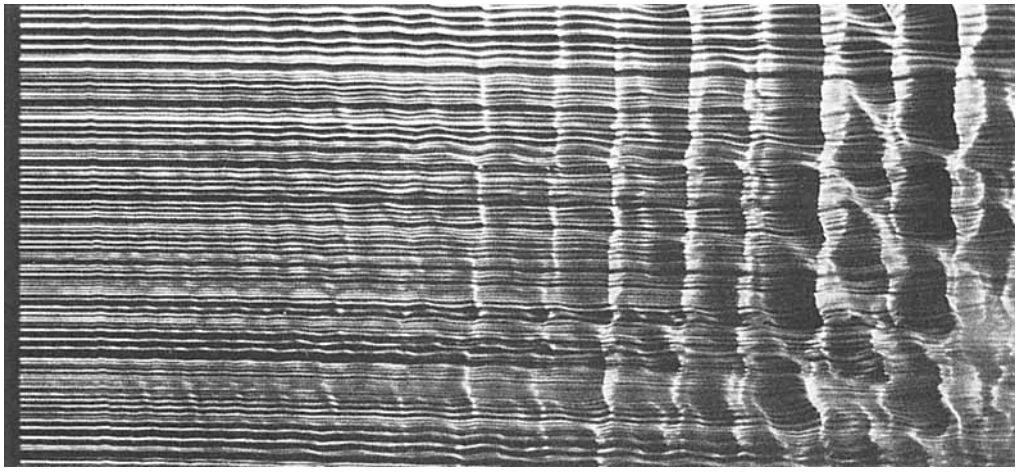

FIGURE 8. Visualization of two-dimensional waves with a spanwise waviness in the far wake, showing the waves at 120 Hz that are due to contamination from our smoke wire AC-DC rectifier. A spanwise waviness on the two-dimensional waves develops downstream due to interaction with the oblique shedding waves from upstream.

difficult, although a fleeting observation on one roll of film had been made at the earliest point in our studies. The reason for our difficulties turned out to be the fact that the smoke wire current was provided by an AC-DC Converter, which retained some small residual AC current. By spectral analysis of the far wake with the smoke wire turned on, we discovered that the far wake was contaminated or 'overpowered' with the smoke wire frequency at 120 Hz. We present, in figure 8, a typical example of smoke visualization at $y/D = 2.0$, and $x/D = 100$, with the original AC-DC rectifier. It should first be noted that the principal waves are parallel, not oblique, and secondly that a spanwise waviness develops, due to the interaction with upstream oblique shedding waves. Thirdly, one may observe that the far-wake spanwise wavelength is equal to the oblique-shedding spanwise wavelength.

With installation of a true DC Power supply, we were able to show immediately a strong and remarkably clear oblique wave resonance in the far wake, as shown in figure 9, and which was the cause of some excitement. The smoke wire has been placed downstream at $x/D = 100$, and the oblique wave angle, in this particular case, is around 26°, which is coincidentally around twice the angle of oblique shedding of 14°.

There remains the possibility that these waves are some artifact of the visualization technique. Such a possibility was made clear in the careful work of Cimbala *et al.* (1988), who demonstrated that the visualization is highly dependent on where the smoke is introduced into the flow. In figure 10, the smoke wire has been placed at different downstream locations, and at a constant $y/D = 2$. If the smoke wire is upstream, we see first the oblique shedding vortices, and further downstream the two-dimensional waves are evident. Based on this picture, one might infer no oblique wave resonance, due to the streakline 'history' effect. However, by placing the smoke wire further downstream at $x/D = 50$, one can now interpret the downstream structure as possibly oblique. When the smoke wire is at $x/D = 150$, there is no question that the far-wake structures are oblique resonance waves. It is clear that the streakline history effect discussed by Cimbala *et al.* is camouflaging the oblique wave resonance when the smoke wire is upstream. The dependence of transverse smoke wire location was also investigated in figure 11, from which we can clearly see the oblique waves when the

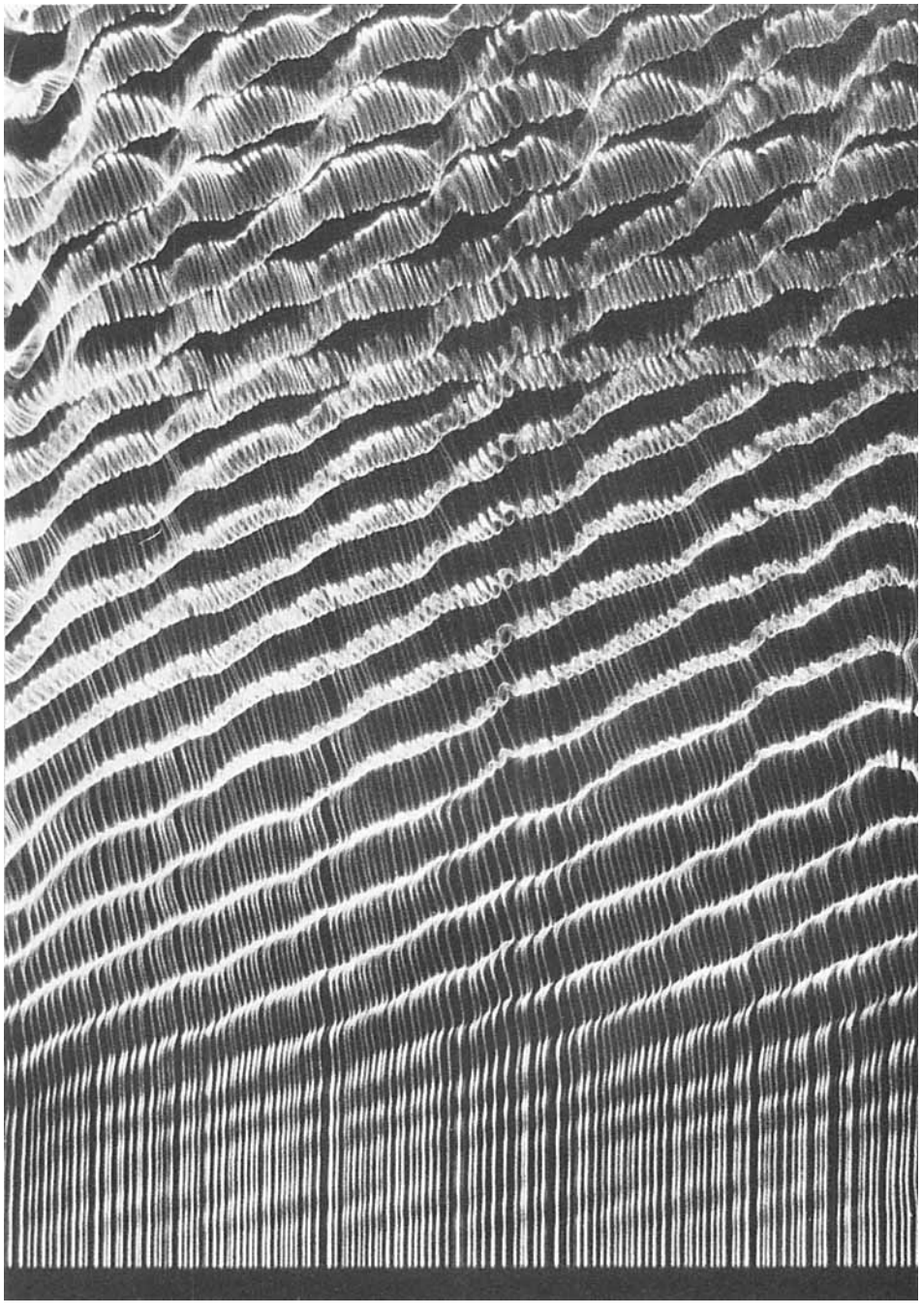

FIGURE 9. Visualization of 'oblique wave resonance' in the far wake. In this photograph, we demonstrate, for the first time, the phenomenon of oblique wave resonance in the far wake, due to nonlinear interaction between oblique shedding waves and large-scale two-dimensional waves. Smoke wire at $x/D = 100$, $y/D = 2.0$.

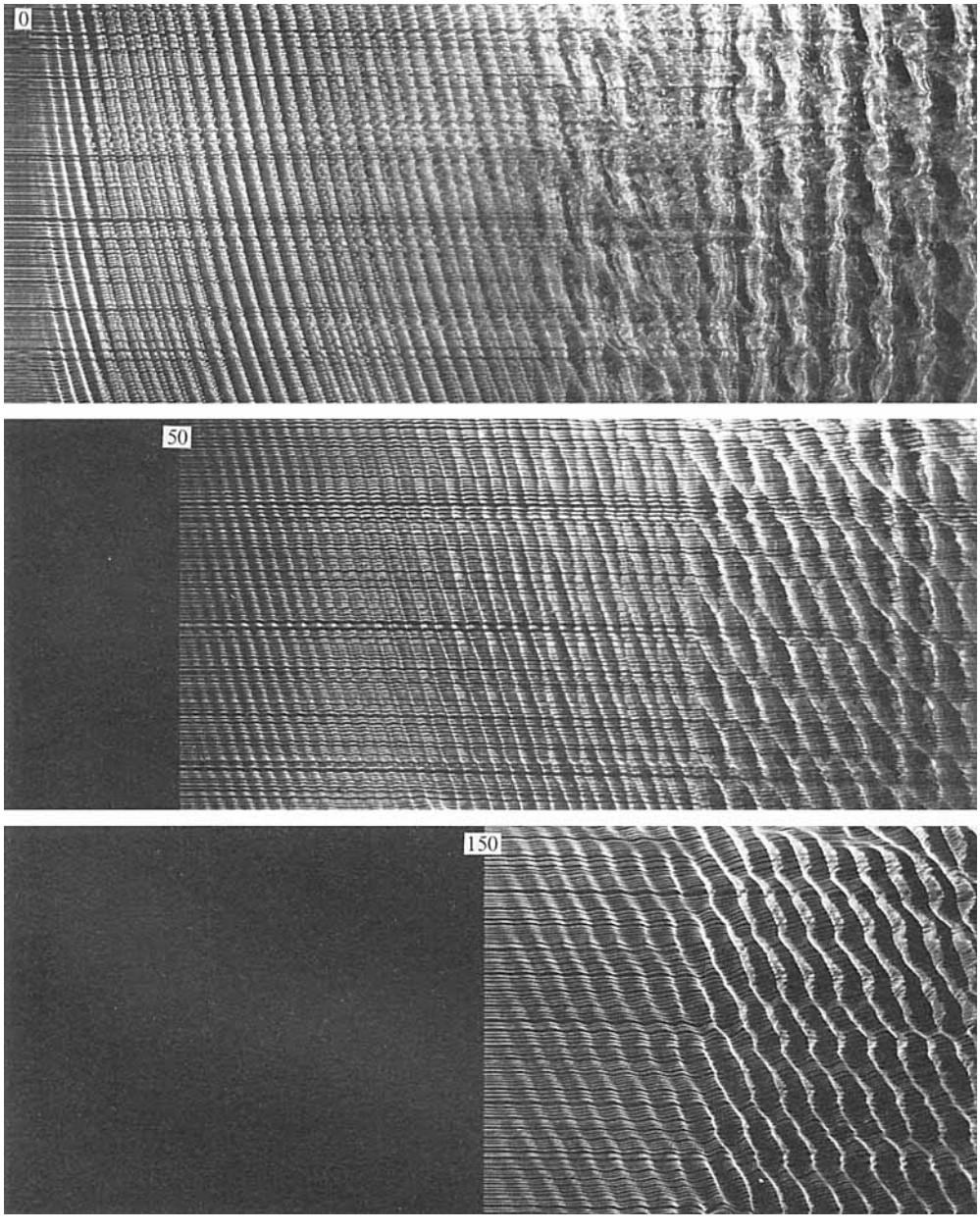

FIGURE 10. Influence of downstream smoke-wire location on oblique-two-dimensional wave interpretation. In the top photograph, with the smoke wire upstream of the cylinder, it appears that the downstream waves are only two-dimensional, due to the streakline history effect. In the middle picture, one can now interpret the downstream structure as possibly oblique. In the last picture, with the smoke wire at $x/D = 150$, there is no question that the far-wake structures are oblique resonance waves. $y/D = 2.0$ for all photographs.

smoke wire is placed at different y/D across the whole wake. One may conclude from the above that the oblique wave resonance is not an artifact of the flow visualization technique.

Measurements of the wavelengths and wave angles made from the visualization

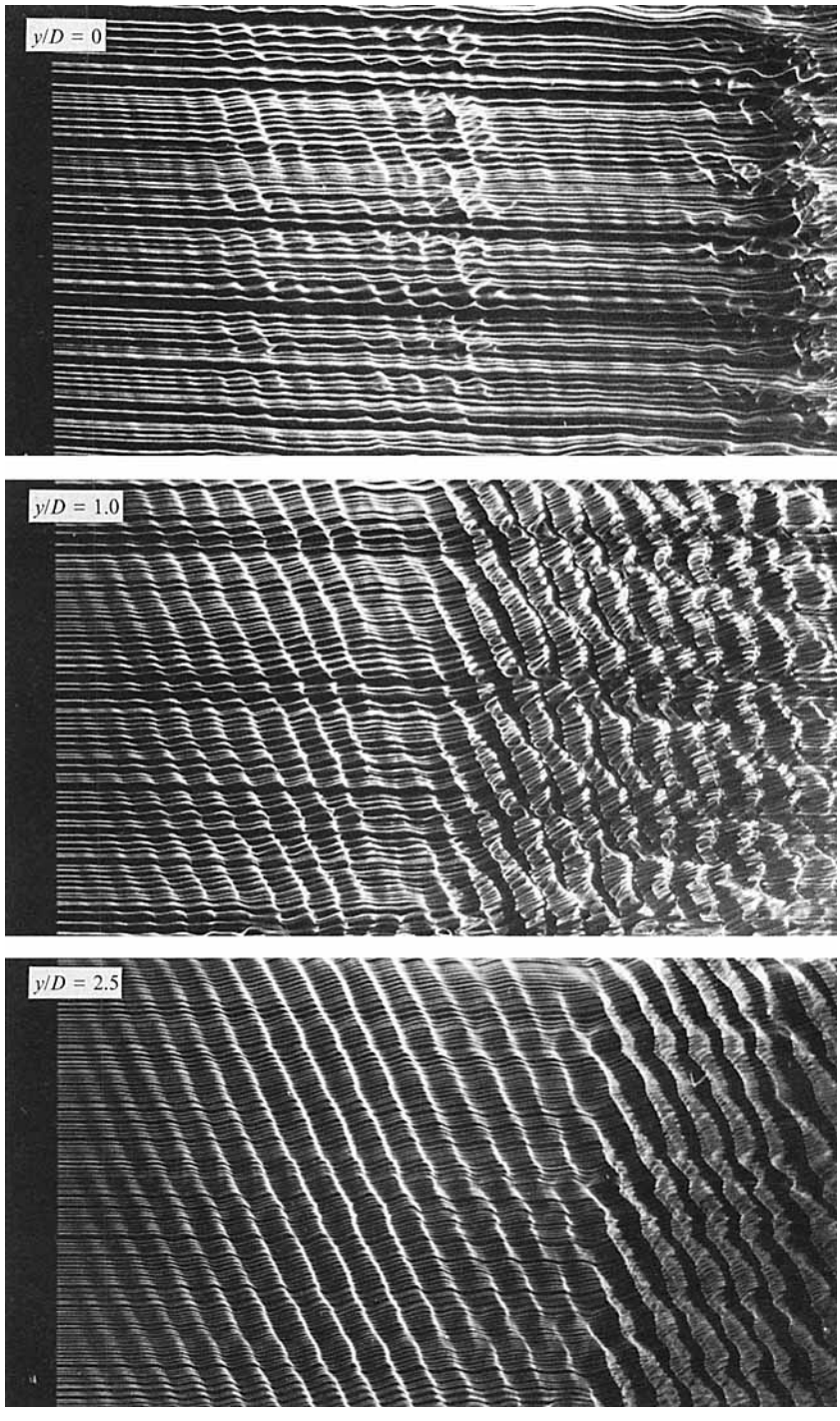

FIGURE 11. Influence of lateral location of smoke wire on oblique wave interpretation. We demonstrate that oblique resonance waves are visualized at all values of y/D. The smoke wire is downstream at $x/D = 100$.

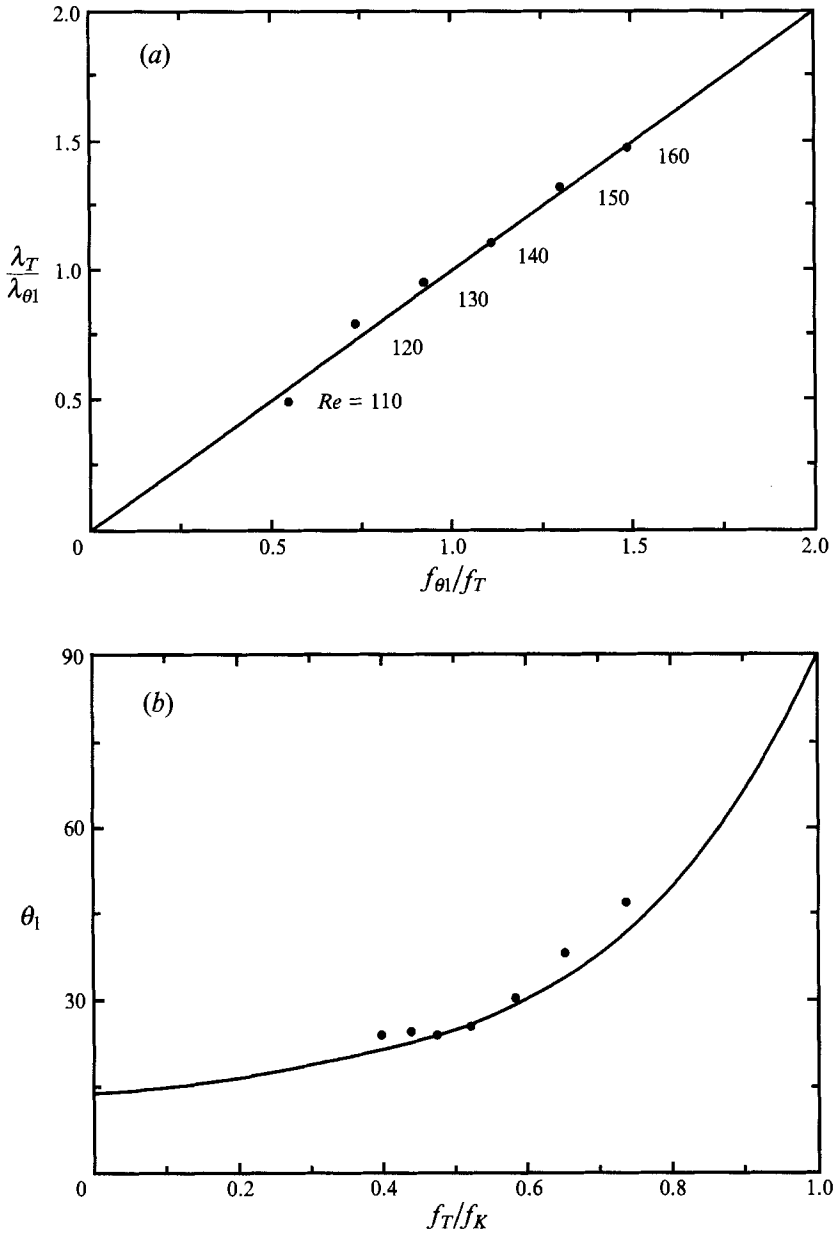

FIGURE 12. Measurements of oblique wave geometry. In (*a*), the measurements show that two-dimensional and oblique waves have equal phase speeds. In (*b*), measurements of oblique wave angles are compared with (predictions based on) equation (15), where θ_K has been taken as 14° over the range of Reynolds number.

pictures are shown in figure 12. For resonance to occur in the manner described from the above equations, the phase speed of the three waves must be equal

$$\lambda_K f_K = \lambda_T f_T = \lambda_{\theta 1} f_{\theta 1}. \tag{16}$$

Although it seemed evident from the pictures that the pattern remained phase-locked

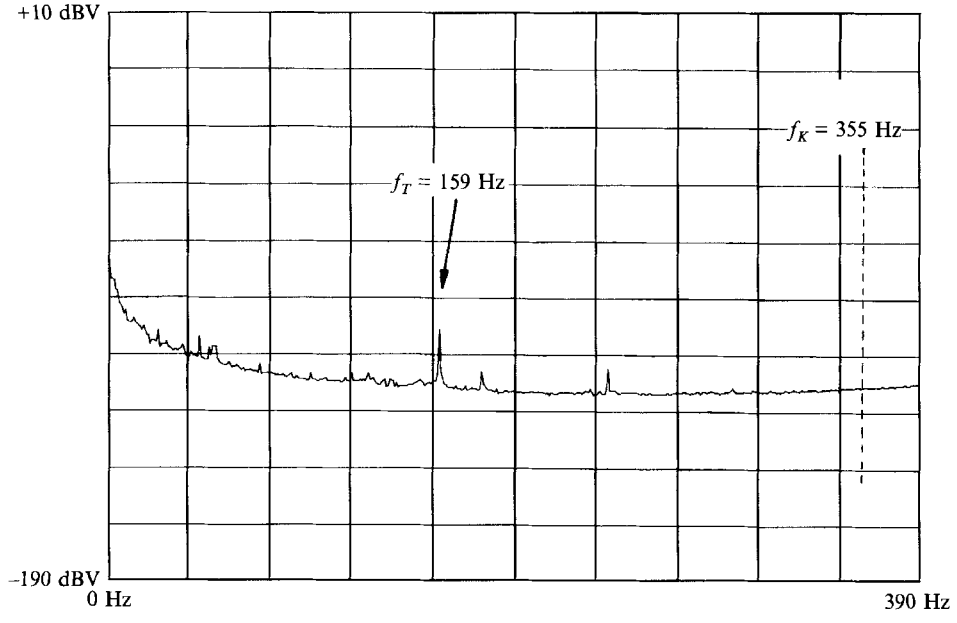

FIGURE 13. Free-stream velocity spectrum ($Re = 150$). The fluctuations at the frequency 159 Hz are given by $(u'_{rms}/U) = 0.00005$, which provides a surprisingly small energy sufficient to trigger the oblique wave resonance.

as it travelled downstream, it was decided to measure the ratio of $(\lambda_T/\lambda_{\theta 1})$ as a function of frequency ratio $(f_{\theta 1}/f_T)$. The plot in figure 12(*a*), showing that the two ratios are equal, demonstrates that the phase speeds of the waves are equal as given in equation (16). Phase-locking was also demonstrated in the three-wave subharmonic interactions of Corke *et al.* (1992), for perturbation amplitude of the two-dimensional waves above a certain threshold.

The measurements of oblique resonance wave angle θ_1 in figure 12(*b*) show a good agreement with predictions based on equation (15). In this case, for simplicity, the oblique shedding angle $\theta_K = 14°$ has been assumed to be constant over the range of Reynolds number. The observed range of (f_T/f_K) in the plot is made possible by a variation in Re over the range 100–160. The plot demonstrates that one may expect oblique resonance for surprisingly large wave angles of at least 50° to the two-dimensional wave. Oblique wave resonance was not evident for Reynolds numbers below about 100; indeed it was difficult to detect any significant far-wake response at Re much below 90–100.

6. Downstream development of velocity fluctuations

It is clear from this investigation, and from the work of Cimbala & Krein (1990), that the far wake is extremely sensitive to the background noise in the free stream. The far wake locks onto combination frequencies of the spectral peaks in the free stream. The free-stream spectrum in the present wind tunnel is shown in figure 13, for a flow speed corresponding to $Re = 150$. The peak at 159 Hz is close enough to the Kármán shedding frequency at 355 Hz to cause the kind of interference leading to oblique wave resonance, although it should nevertheless be realized that the energy at this fluctuation

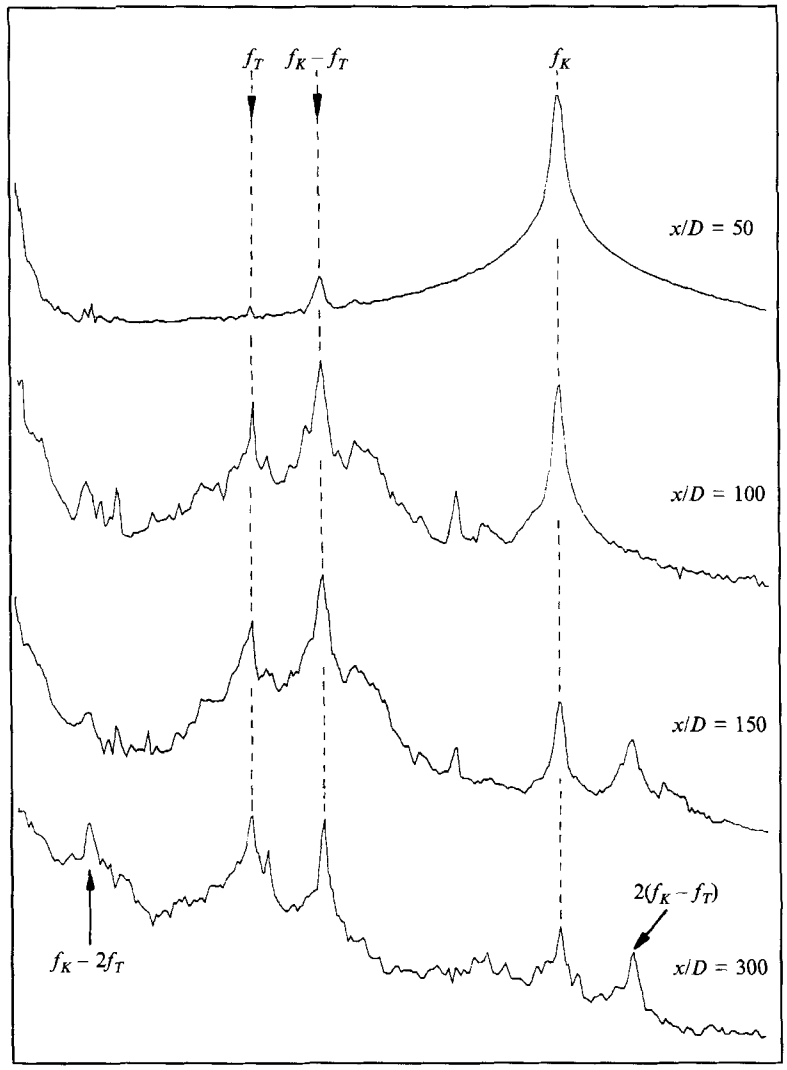

FIGURE 14. Development of velocity spectra downstream ($Re = 150$). The spectral peak at $(f_K - f_T)$ in the far wake is the dominant peak, until around $x/D = 300$, when the peak at (f_T) becomes comparable.

peak is remarkably low, giving a value of $(u'_{rms}/U) = 0.00005$. One may note for comparison that the near-wake fluctuation levels are of order $(u'_{rms}/U) = 0.20$.

Downstream developments of velocity spectra for $Re = 150$ are shown in figure 14. The energy of the oblique resonance waves $(f_K - f_T)$ exceeds that for the oblique shedding waves (f_K) at around $x/D = 90$, and is much larger by $x/D = 150$. It should be noted that, under these particular conditions, the energy for the parallel waves (f_T) also grows downstream to be comparable to the oblique resonance waves $(f_{\theta 1})$ around $x/D > 300$. We might expect this to occur because $f_T < f_{\theta 1}$, and the band of amplified frequencies would be expected to shift to lower frequencies as the wake progresses downstream, as indicated by Cimbala *et al.* (1988). Also noticeable in the spectra at $x/D = 150$ and 300 is a peak at $2f_{\theta 1}$, which is the harmonic of the oblique resonance wave, and a further peak at the combination frequency $(f_K - 2f_T)$ which will be shown in Williamson & Prasad (1993*b*) to represent a further oblique resonance mode.

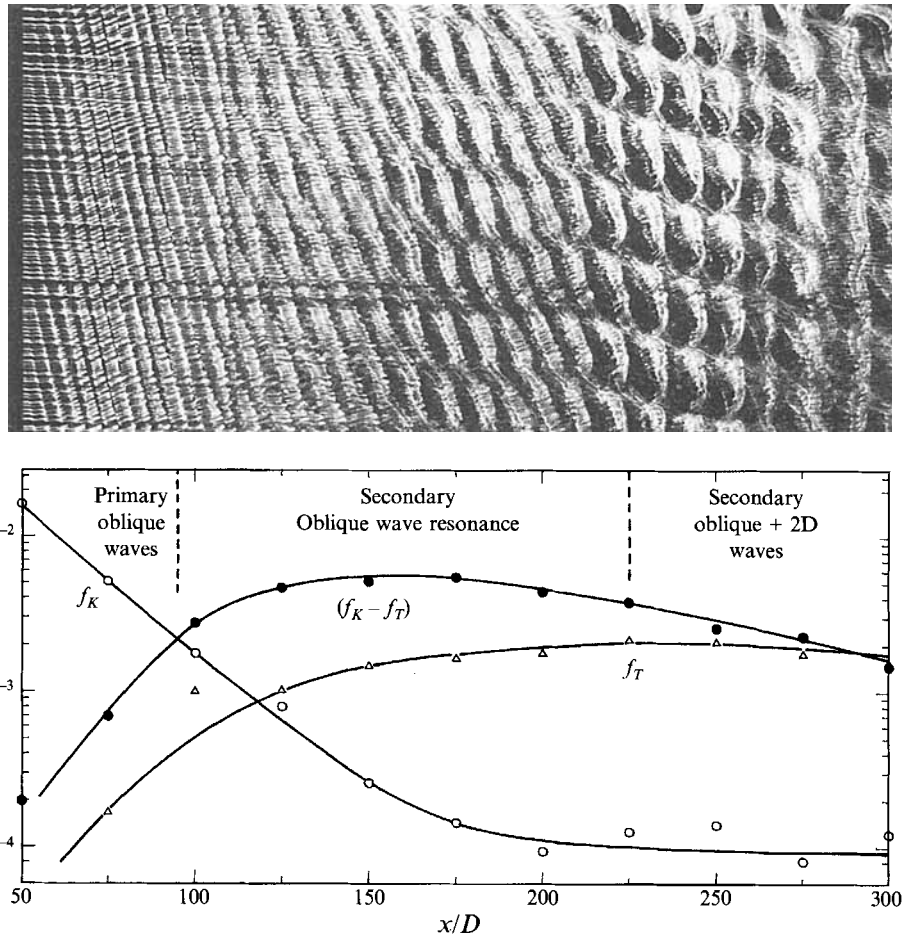

FIGURE 15. Development of velocity fluctuations downstream ($Re = 150$). The downstream distance in the visualization is to-scale with the measurements below. The smoke wire was placed at $x/D = 50$, in order to show all three sets of waves. The measurements of (u'_{rms}/U) show the exponential decay of Kármán vortices, the growth of oblique resonance waves, and further downstream a comparable mix of two-dimensional and oblique waves (comprising a honeycomb pattern).

Corresponding flow visualization and fluctuation measurements are shown (to the same x/D scale) in figure 15. These velocity r.m.s. measurements were obtained from the maximum value found across the wake noted from an RMS voltmeter, so there is no preference for any specific frequency. The smoke wire is situated at $x/D = 50$ in order to show all three sets of waves in one picture. The oblique shedding vortices may be seen giving way to the oblique resonance waves as one moves downstream to the right. There is a region of interaction further downstream, involving both the oblique resonance waves and the large-scale two-dimensional waves, and so a honeycomb pattern is observed. The observations are reflected also in the measurements.

At this point, we introduce in figure 16 some precise definitions regarding the near and far wakes. The near wake is defined as the region of growing velocity fluctuations, until reaching a peak at what is commonly known as the formation length, X_F. In this study, we shall define the far wake as the region downstream of the point at which the

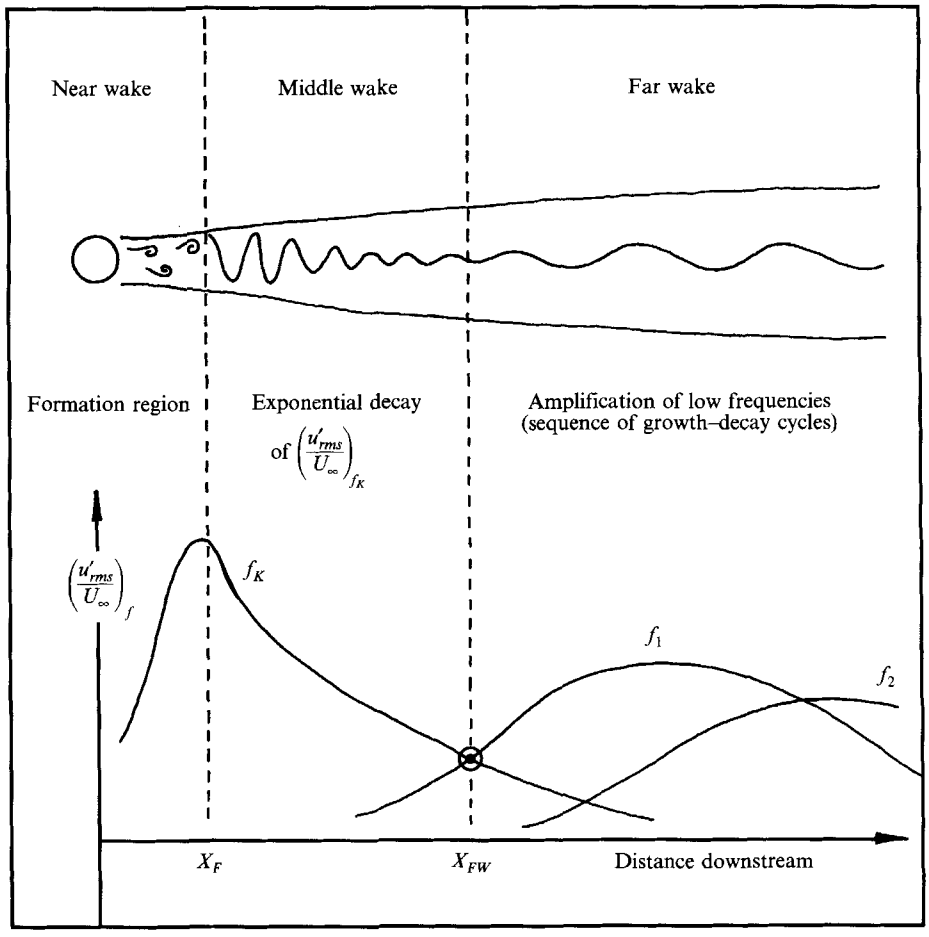

FIGURE 16. Definition of downstream wake regions: the far wake is defined as the region downstream of the position (X_{FW}) where the fluctuations from the decaying Kármán vortices and the growing far-wake waves are equal.

decaying energy of the shed vortices is equal to the growing energy of the amplified modes in the far wake, which will be called the far-wake distance, X_{FW}. The intermediate region, which is characterized by the exponential decay of the shed vortices, is defined as the middle wake. This far-wake distance defines a point at which one may compare fluctuation energy for different conditions. In figure 17(*a*), the far-wake distance X_{FW} is shown to decrease as Reynolds number increases, in roughly a $1/Re$ dependence. The strength of the fluctuations at this characteristic point in (*b*) increases with Reynolds number. These characteristic values will be used for comparison with different experimental conditions in §8.

7. Modes of oblique wave resonance

A revealing plot of the far-wake frequencies is shown as the normalized frequency (f/f_K) versus Re in figure 18. In this plot it can be seen that for all the laminar regime down to near $Re = 90$, the data fall on the oblique resonance curve, given by $(1-f_T/f_K)$. It should be noted that this plot is specific to the particular frequency corresponding to $(f_T D^2/\nu) = 12.0$. Of particular significance is that the wake frequency

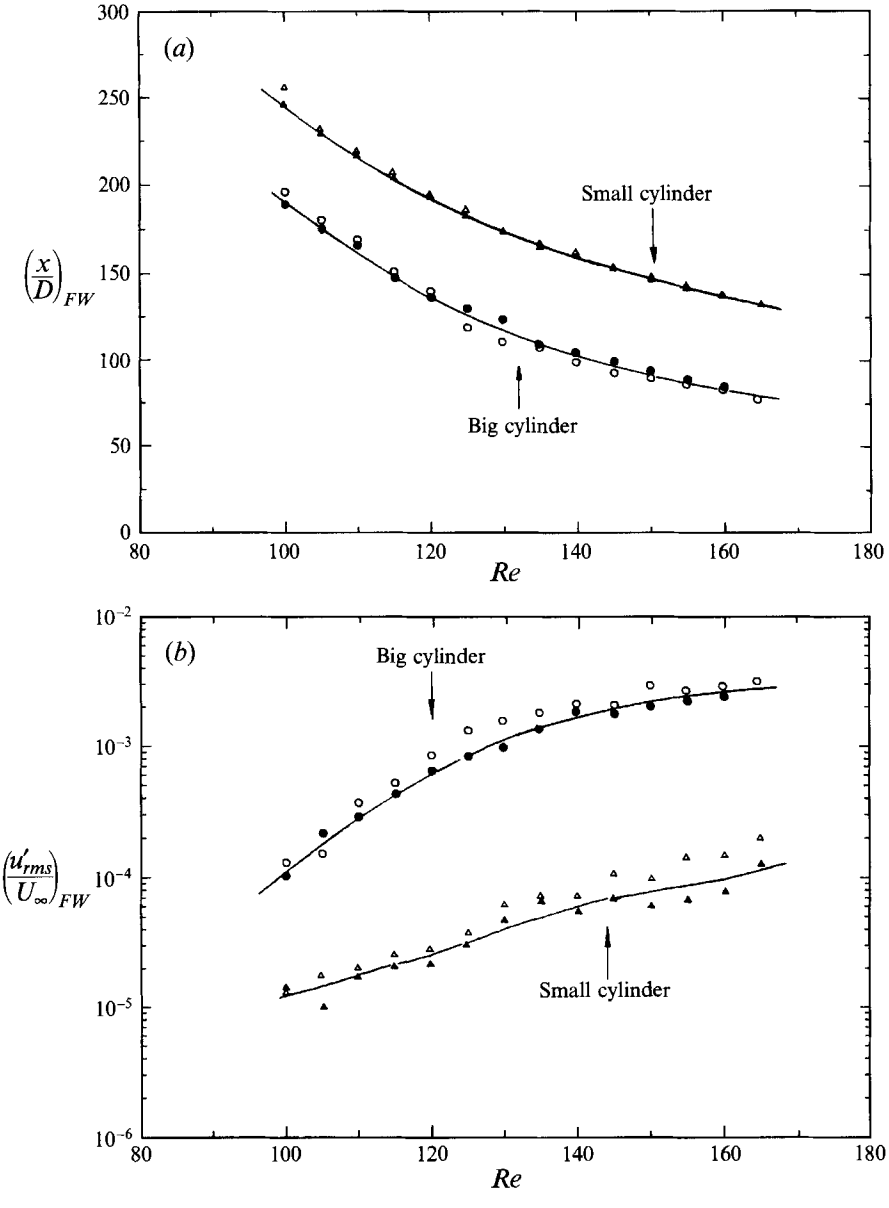

FIGURE 17. Measurements of (*a*) normalized far-wake distance $(x/D)_{FW}$ and (*b*) velocity fluctuations at $(x/D)_{FW}$ in, versus *Re*. Solid symbols are for oblique shedding, and open symbols are for parallel shedding. The circles refer to the large cylinder, and the triangles refer to the small cylinder.

response follows the oblique waves curve, even when the oblique and two-dimensional frequencies are closely comparable near $Re = 134$, at which point $f_T/f_K = \frac{1}{2}$. There is clearly a preferential amplification of oblique resonance waves over the two-dimensional waves throughout the range of wake response.

The plot in figure 18 shows that the oblique wave frequency ($f_{\theta 1}$) is greater than the two-dimensional wave frequency (f_T) for $Re > 134$, or $f_T/f_K < \frac{1}{2}$. This suggests that, if there is initially a preferential oblique wave amplification, then further downstream, as the receptivity of the wake shifts to lower values of frequency, the two-dimensional

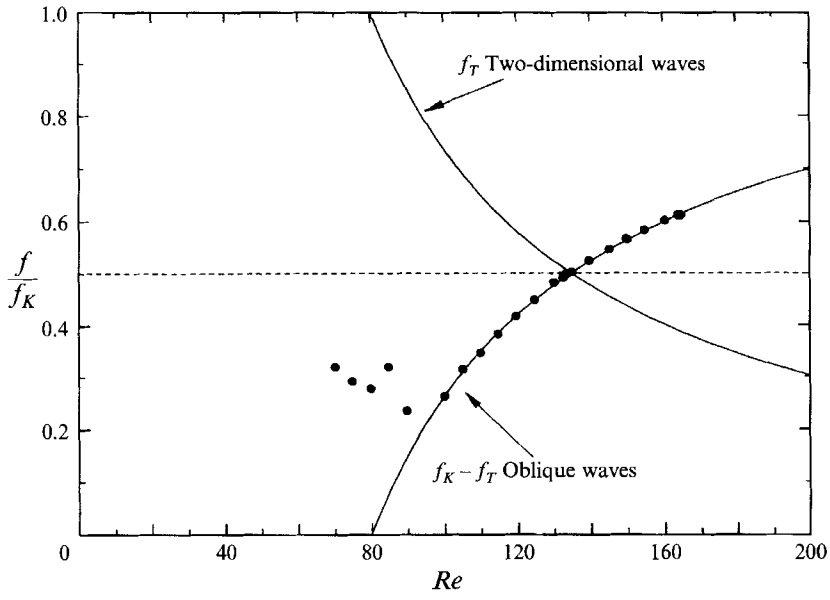

FIGURE 18. Normalized far-wake frequency (f/f_K) versus Re: preferential amplification of oblique waves. The two-dimensional waves curve and oblique waves curve are drawn using ($f_T D^2/\nu$) = 12.0.

waves may become amplified also. On the other hand for $f_T/f_K > \frac{1}{2}$, if the oblique waves are preferentially amplified initially, then one may not expect the two-dimensional waves of higher frequency to amplify or become comparable further downstream. There are thus two possible modes of oblique waves resonance, in this case, as follows:

Oblique mode:	$f_{\theta 1} < f_T$,	$f_T/f_K > \frac{1}{2}$,	$Re < 134$
Oblique–Two-dimensional mode:	$f_{\theta 1} > f_T$,	$f_T/f_K < \frac{1}{2}$,	$Re > 134$.

The example discussed in the previous section for $Re = 150$ corresponds to $f_{\theta 1} > f_T$, and therefore to the Oblique–Two-dimensional mode, resulting in a combination of waves as for the 'honeycomb' pattern. In the present section, we present evidence of the Oblique mode, commencing with the spectral development in figure 19. In this case $Re = 120$, corresponding to $f_{\theta 1} < f_T$, and it is clear that, although the parallel waves (f_T) are involved in triggering the oblique wave resonance at around $x/D = 100$, they are lost in the background noise at $x/D = 300$, whereas the oblique waves ($f_K - f_T$) are still relatively energetic. Measurements of velocity fluctuation in figure 20 demonstrate similarly the exponential decay of Kármán waves, the small growth and decay of the parallel waves (f_T), and the relatively much larger amplification of oblique resonance waves ($f_K - f_T$). There is no appearance of comparable parallel waves further downstream, in this instance. Visualization in figure 21, where the smoke is introduced at $x/D = 100$, shows the two modes, depending on whether $Re \lessgtr 134$.

8. Experiments with a smaller cylinder: very low free-stream interference

The results to this point demonstrate not only the phenomenon of oblique wave resonance, but also an extreme sensitivity of the far wake to any small peaks in the free-

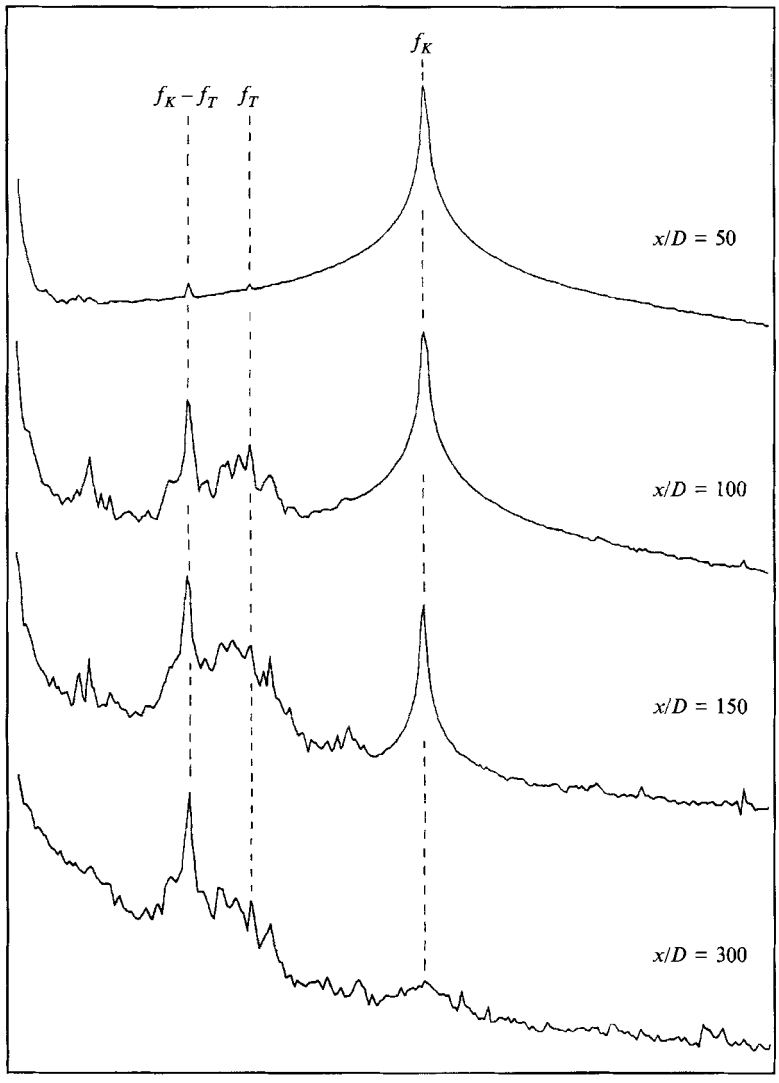

FIGURE 19. Development of spectra downstream, $Re = 120$: oblique resonance mode. In this case the oblique resonance waves at frequency $(f_K - f_T)$ remain far more energetic than the two-dimensional waves (f_T), which do not appear further downstream.

stream spectrum. The response of the far wake is dependent on the frequency as well as the amplitude of any background noise. In this section, we shall investigate experimental conditions for which the noise not only has less amplitude, but where the frequency peak (f_T) is placed an order of magnitude away from the typical Kármán shedding frequency (f_K). In this way, one would be likely to avoid interference from both the direct frequency (f_T) and the combination frequency $(f_K - f_T)$. For this purpose, a smaller cylinder of 0.53 mm diameter was used, so that the shedding frequency would be typically over four times higher than for the original cylinder. The following data for the two cylinders relate to conditions at $Re = 150$:

Larger cylinder ($D = 1.08$ mm) $(u'_{rms}/U)_{f_T} = 0.005\%$ f_T is around $0.5 f_K$,

Smaller cylinder ($D = 0.53$ mm) $(u'_{rms}/U)_{f_T} = 0.003\%$ f_T is around $0.1 f_K$.

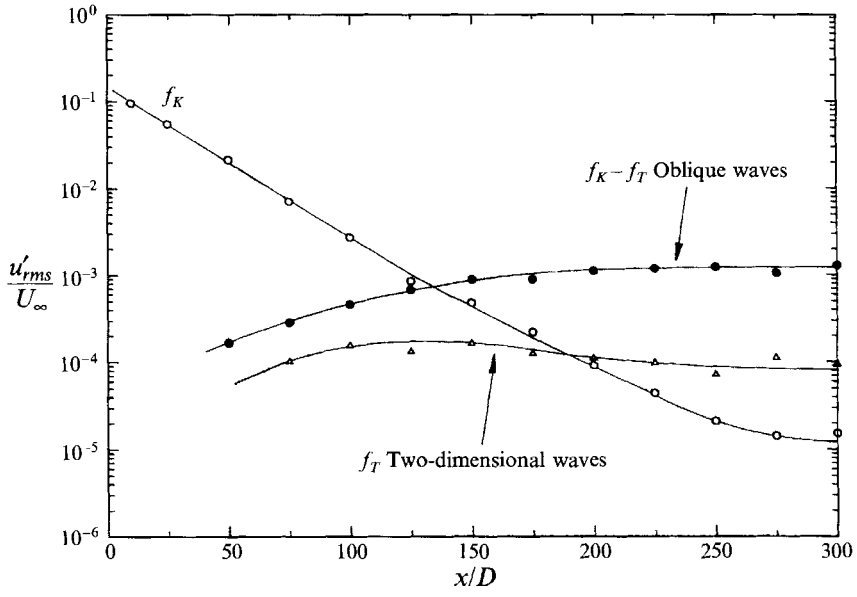

FIGURE 20. Development of velocity fluctuations downstream, $Re = 120$: oblique resonance mode. As shown in the spectra, the oblique resonance waves at frequency $(f_K - f_T)$ remain far more energetic than the two-dimensional waves (f_T). Oblique waves only are observed in the visualizations.

Measurements of the free-stream spectrum for the small cylinder demonstrated an extremely low level of noise, and absence of any peaks in the vicinity of the shedding frequency. The central question is now: what happens to the far-wake wave interactions if the free-stream noise frequency is far from the Kármán shedding frequency?

The spectra for the smaller cylinder presented in figure 22 show a much lower wake response relative to the larger cylinder wake. This is made very clear if one compares the response for $Re = 120$ at $x/D = 150$ with figure 19, and also the response for $Re = 150$ at $x/D = 150$ with figure 14. The character of the far-wake spectral response is also of a broadband nature with no predominant peaks.

An interesting result appears when one plots the normalized far-wake frequency (f_{FW}/f_K) versus Re, in figure 23. The curves for two-dimensional waves (f_T) and oblique wave resonance $(f_K - f_T)$ have been drawn in the figure (corresponding, in this case, to $(f_T D^2/\nu) = 3.0$). The measured wake response frequencies were evaluated as the maximum of a broad region of spectral response, rather than any specific peak, and were found using a polynomial fit through this region. It appears that the response frequency is close to the subharmonic $(f_{FW}/f_K) = \frac{1}{2}$, which is markedly different from the far-wake resonance of the large cylinder. It would be tempting to suggest that, without some resonance with a particular frequency in the free stream, the wake prefers the $\frac{1}{2}$ subharmonic. Whether this is perhaps a coincidence, or whether it provides evidence for a vortex pairing phenomenon are obvious questions, and are pursued in §11.

The downstream development of velocity fluctuations for the small cylinder are shown in figure 24, for $Re = 120$ and 150, and it is seen that there is a drastic reduction in far-wake response compared to the large cylinder shown in figures 15 and 20, and overlaid as the curves in this figure. There is at least a factor of 10 reduction in far-wake fluctuations for $Re = 150$, and a factor of 100 in the case of $Re = 120$. Following the

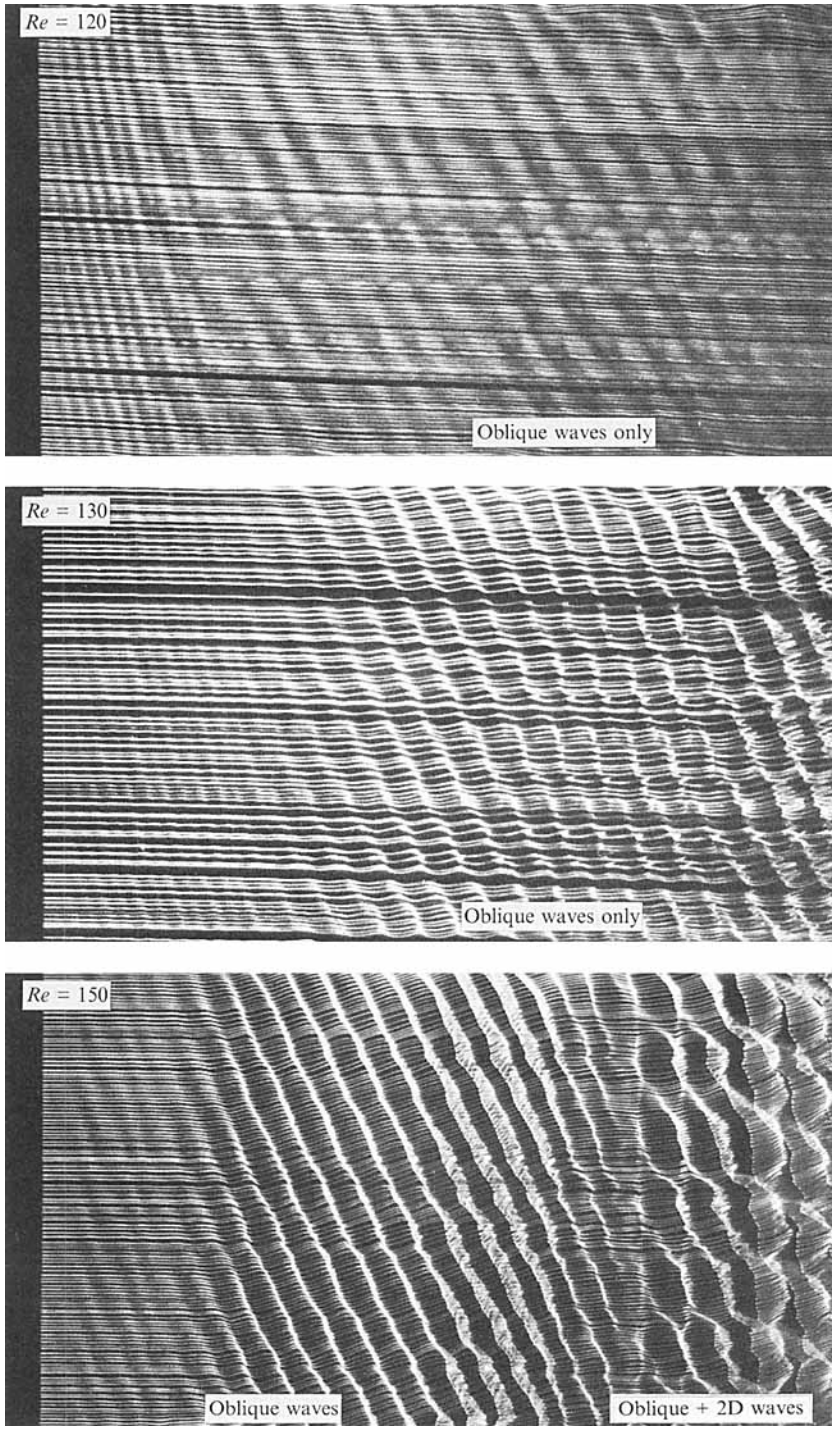

FIGURE 21. Visualisation of the two modes of oblique wave resonance, when $f_T/f_K \lesseqgtr \frac{1}{2}$. In this case, the two modes are found for $Re \gtrless 134$. The photographs extend from $x/D = 100$ to 320.

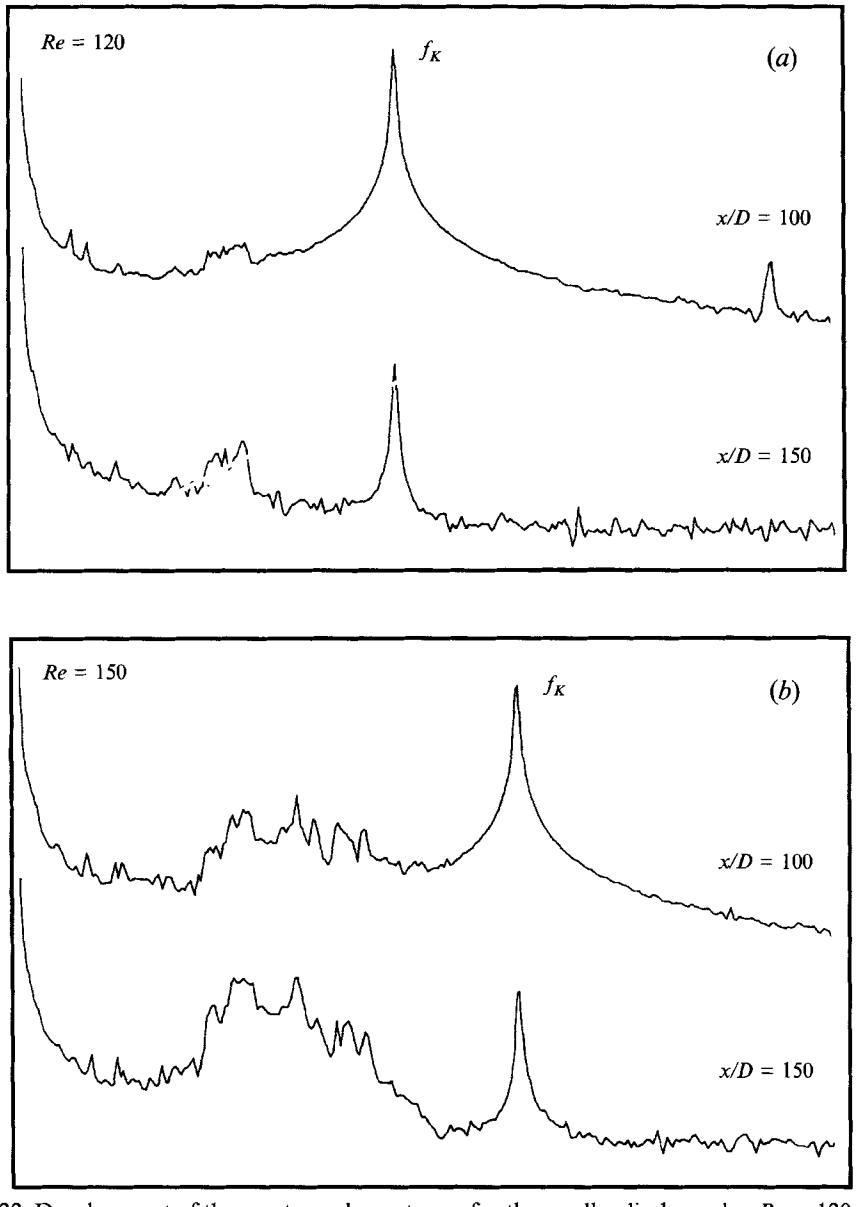

FIGURE 22. Development of the spectrum downstream for the small-cylinder wake, $Re = 120$ and 150. This non-resonant response in the far wake is broad and low amplitude, and may be contrasted with the larger spectral peaks in the resonant wake of the larger cylinder.

earlier definition of far-wake distance, this characteristic length versus Re has been plotted for the small cylinder wake in figure 17 earlier, demonstrating the much larger distance $(x/D)_{FW}$, and the much lower fluctuations $(u'_{rms}/U)_{FW}$ at this characteristic point for the small cylinder wake as compared with the large cylinder wake. Finally, some flow visualization at $Re = 150$ in figure 25, using smoke introduced at $x/D = 100$ and $y/D = 1.5$, demonstrates the remnants of the oblique shedding waves at the left, and very little structure at all in the far wake. This suggests that the regular patterns observed up to now in far wakes (honeycomb pattern and oblique or two-dimensional

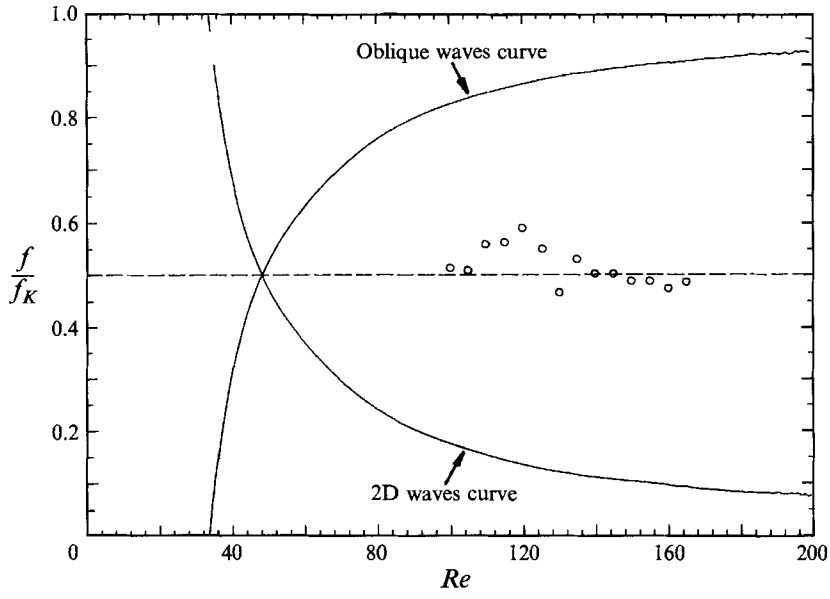

FIGURE 23. Normalized far-wake frequency (f/f_K) versus Re: no amplification of oblique waves. The two-dimensional-waves curve and oblique-waves curve are drawn using $(f_T D^2/\nu) = 3.0$.

wave patterns) are indicative of a response to specific frequency peaks in the free-stream spectrum.

9. Comparison with predictions from linear stability analysis

Although the oblique wave resonance is a nonlinear phenomenon, it is nevertheless possible to make some useful comparisons between the present phenomena and predictions based on linear stability analysis. Cimbala (1984) and Cimbala *et al.* (1988) conducted a comparison of measured far-wake frequencies with those frequencies predicted on the basis of spatial inviscid linear stability of a parallel Gaussian wake profile. We shall show, for the same $Re = 150$, that our far-wake velocity profiles are closely similar to those measured by Cimbala *et al.*, and subsequently we will utilize their theory to compare with some of the present results.

We have found a very reasonable agreement of the mean velocity profiles with a Gaussian form, for downstream positions extending from around $x/D = 20$ to beyond $x/D = 300$. In such a profile, a normalized wake velocity defect may be given by

$$U^* = \frac{U - U_\infty}{U_0 - U_\infty}, \tag{17}$$

where U_0 is the centreline velocity. A normalized transverse distance can be given as $y^* = y/\delta$, where δ is the wake half-width defined by that value of y for which $U^* = 0.5$. The downstream development of both the normalized maximum velocity defect $W_0/U_\infty = (U_\infty - U_0)/U_\infty$ and also the wake width δ/D are plotted in figure 26 for $Re = 150$, and are compared with the results of Cimbala (1984). The agreement in both cases was considered sufficiently close to enable us to use the stability analysis mentioned above. Regarding the plots, it is interesting to note that the wake defect

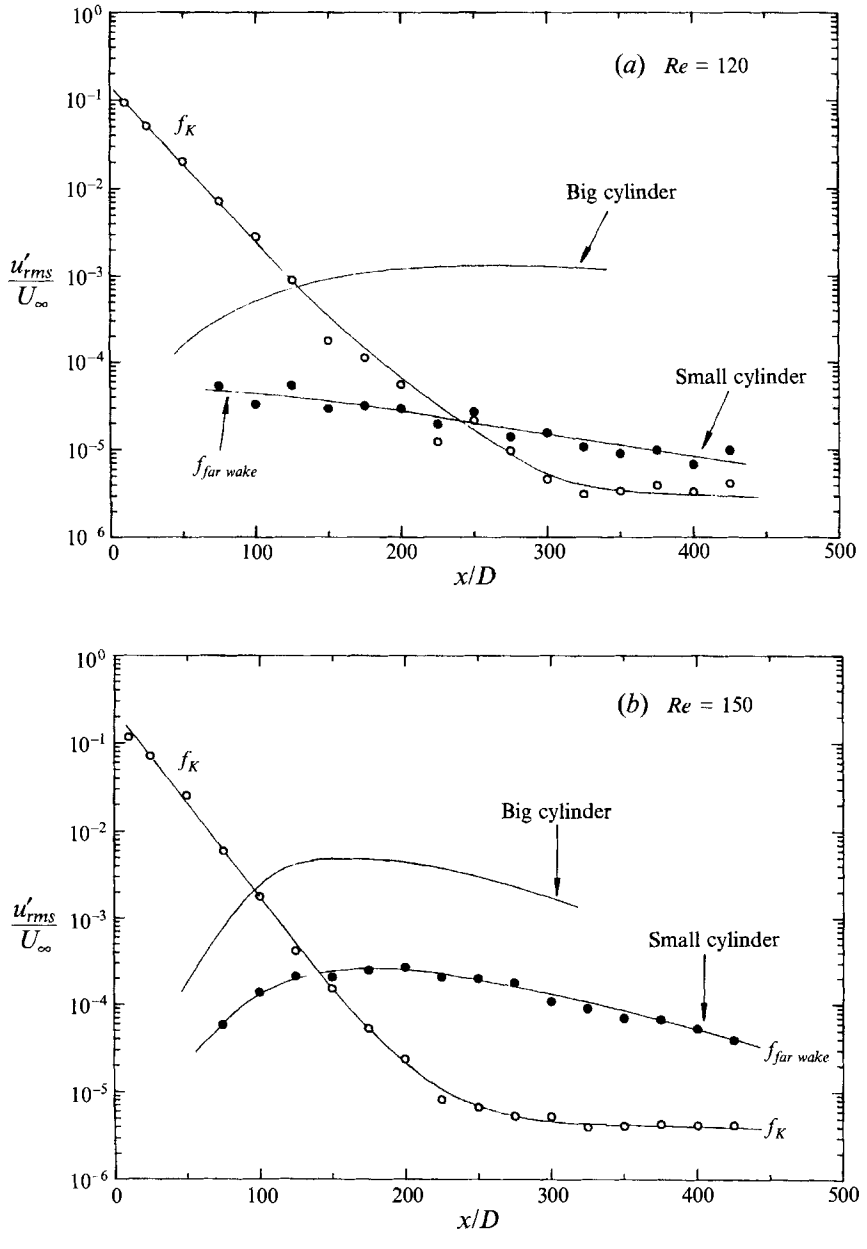

FIGURE 24. Development of velocity fluctuations downstream for the small cylinder. (*a*) $Re = 120$; (*b*) 150. The data for the small-cylinder wake are compared with the much greater fluctuations of the larger-cylinder wake.

(W_0/U_∞) increases for a surprisingly large distance downstream (up to $x/D = 50$), and the expected asymptotic decay following an $x^{-\frac{1}{2}}$ law cannot be reasonably applied until beyond $x/D = 100$. The varying rate of increase of wake width δ is a characteristic that was observed by Cimbala and also by Corke *et al.* (1992), and is possibly related with the decay and growth of different modes.

Profiles of velocity fluctuation at different downstream stations in figure 27 demonstrate that the oblique-wave fluctuations in the far wake exceed the two-

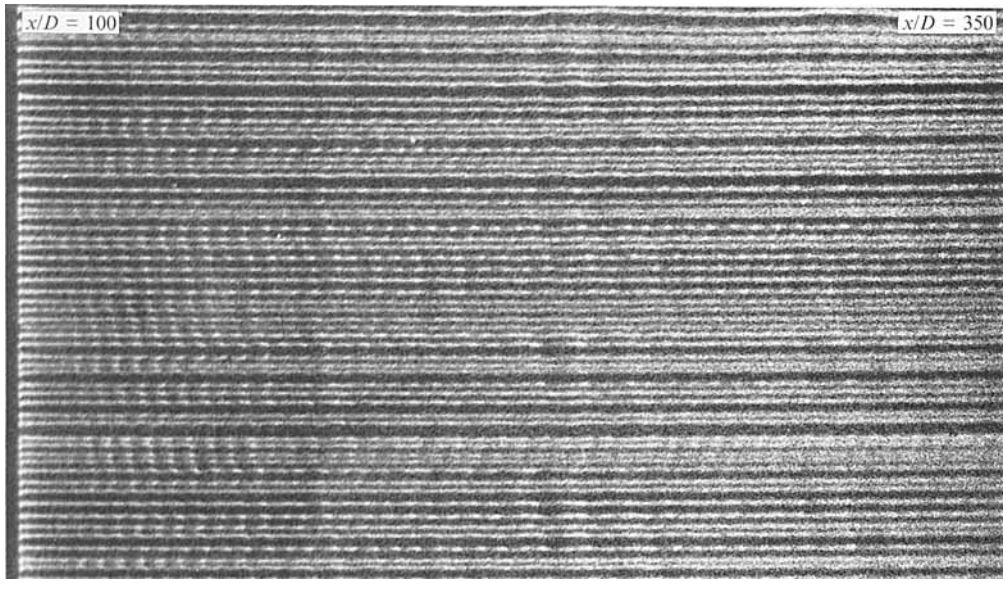

FIGURE 25. Visualization of far wake of the small cylinder, $Re = 150$. This photograph does not show any clear structure in the far wake. The oblique shedding waves are seen to the left.

dimensional wave fluctuations across the complete wake profile (distinctly so at $x/D = 150$), which further confirms the existence of the oblique wave resonance. However, it can be seen that for this Oblique–Two-dimensional Mode ($f_T/f_K < \frac{1}{2}$), the fluctuations for the two sets of waves becomes more comparable further downstream at $x/D = 250$. It should be noted that for $x/D = 150$ and 250, the profile for negative y is the mirror of that for positive y, because there existed a distinct repeatable asymmetry in the measurements. It seemed that, since the larger peak was always on the left side of the plot (to the measurement accuracy) for a whole set of downstream locations, the probe crossing the wake centreline affected this sensitive measurement, in agreement with Desruelle (1983).

A comparison of measured and predicted frequencies in the far wake is presented in figure 28. The stability curves in this figure are as drawn by Cimbala *et al.* (1988). The 'neutral' curve defines those frequencies below it as unstable. There is a further curve defining frequencies with the 'maximum growth' rate, based on a local wake-profile analysis. The solid curve defines a predicted prominent frequency, using a locally parallel scheme, but which takes into account the integrated growth of disturbances with downstream distance. For the large cylinder in (*a*), the predominant frequency falls in steps from the Kármán frequency (f_K) to the oblique resonance frequency ($f_K - f_T$), and then to the parallel waves frequency (f_T) near $x/D = 300$. Like Cimbala *et al.*, the energy at a given frequency grows until it reaches the neutral curve, after which it decays and a further lower frequency takes over as the most amplified one, thus there are growth and decay cycles for different frequencies. The frequencies for the small cylinder in (*b*) do not exhibit pronounced step changes as for the resonant wake in (*a*), and seem to drop in a more continuous fashion. Frequencies, in the resonant and non-resonant cases, fall in the region between the predicted curve and the neutral stability curve, which is consistent with Cimbala *et al.*

The incidence of resonance or non-resonance is also consistent with predictions based on the linear theory. In figure 29, we show the normalized frequency (f_{FW}/f_K)

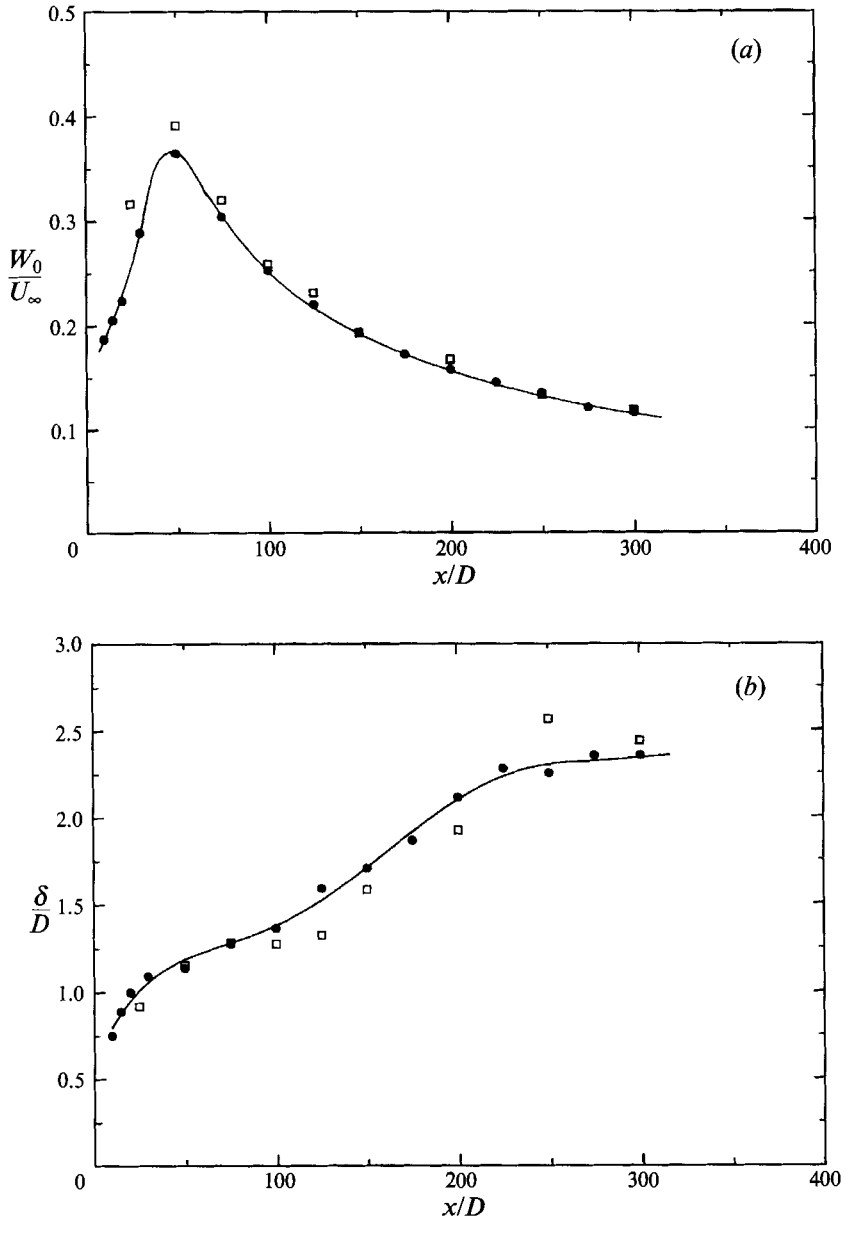

FIGURE 26. Downstream development of normalized wake defect (W_0/U) in (*a*), and normalized wake half-width (δ/D), $Re = 150$: ●, present data; □, Cimbala (1984).

versus Re, for both cylinders. In these figures are drawn the curves corresponding to the oblique or two-dimensional waves, and also curves deduced from the stability calculations. The neutral and maximum-growth curves have been found using the curves of growth rate versus $\beta = 2\pi\delta f/U_\infty$ in figure 12 of Cimbala *et al.*, which are a function of the defect velocity W_0/U_∞. In order to find a reasonable characteristic point in the far wake to conduct stability calculations over a range of Re, it seems reasonable to select the far-wake distance $(x/D)_{FW}$ for the large and small cylinder wakes (figure 17). The data of Desruelle (1983) for $(W_0/U_\infty)_{FW}$, corresponding to these values of

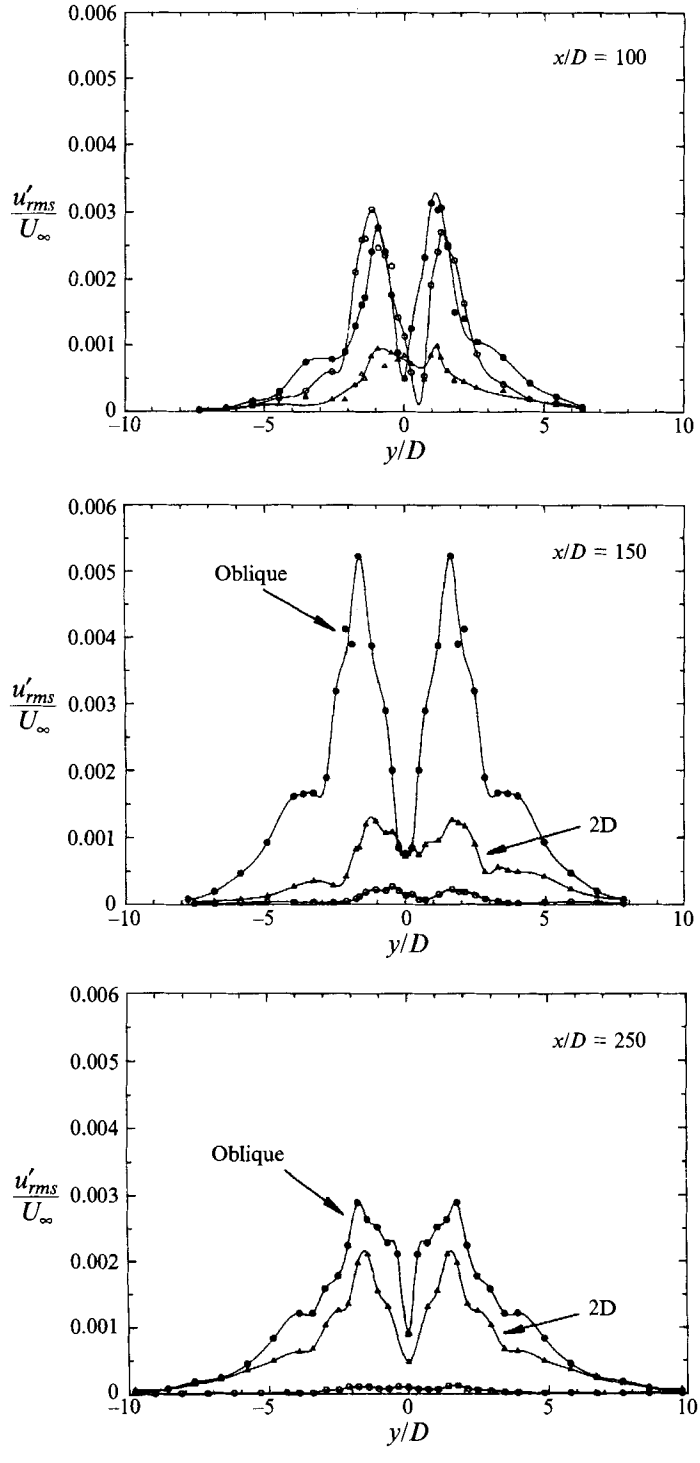

FIGURE 27. Downstream development of profiles of (u'_{rms}/U) versus y/D, $Re = 150$: ●, data for the oblique resonance waves at frequency $(f_K - f_T)$; ▲, the two-dimensional waves at frequency (f_T); ○, the oblique shedding waves at frequency (f_K).

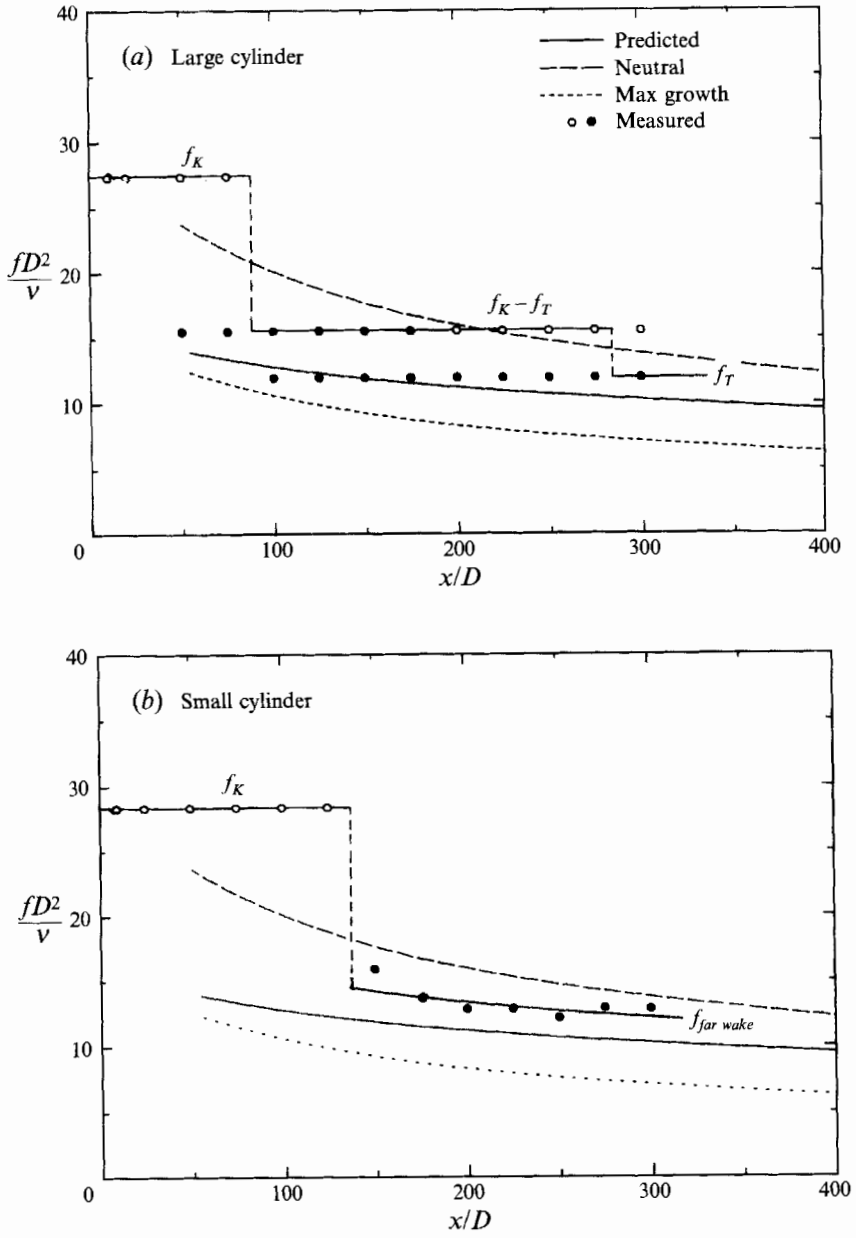

FIGURE 28. Measured and predicted far-wake frequencies versus x/D, $Re = 150$. The curves are from the linear stability analysis of Cimbala *et al.* (1988). The solid symbols refer to a frequency whose energy is growing with respect to downstream distance, while the open symbols refer to decaying waves.

$(x/D)_{FW}$, are used to interpolate values for β from the curves of Cimbala *et al.* The data for β, and the data for $(\delta/D)_{FW}$ also from Desruelle, as well as present measurements of Strouhal number S_K, are then used in the equation

$$\frac{f}{f_K} = \frac{\beta}{2\pi} \frac{1}{(\delta/D)_{FW}} \frac{1}{S_K} \tag{18}$$

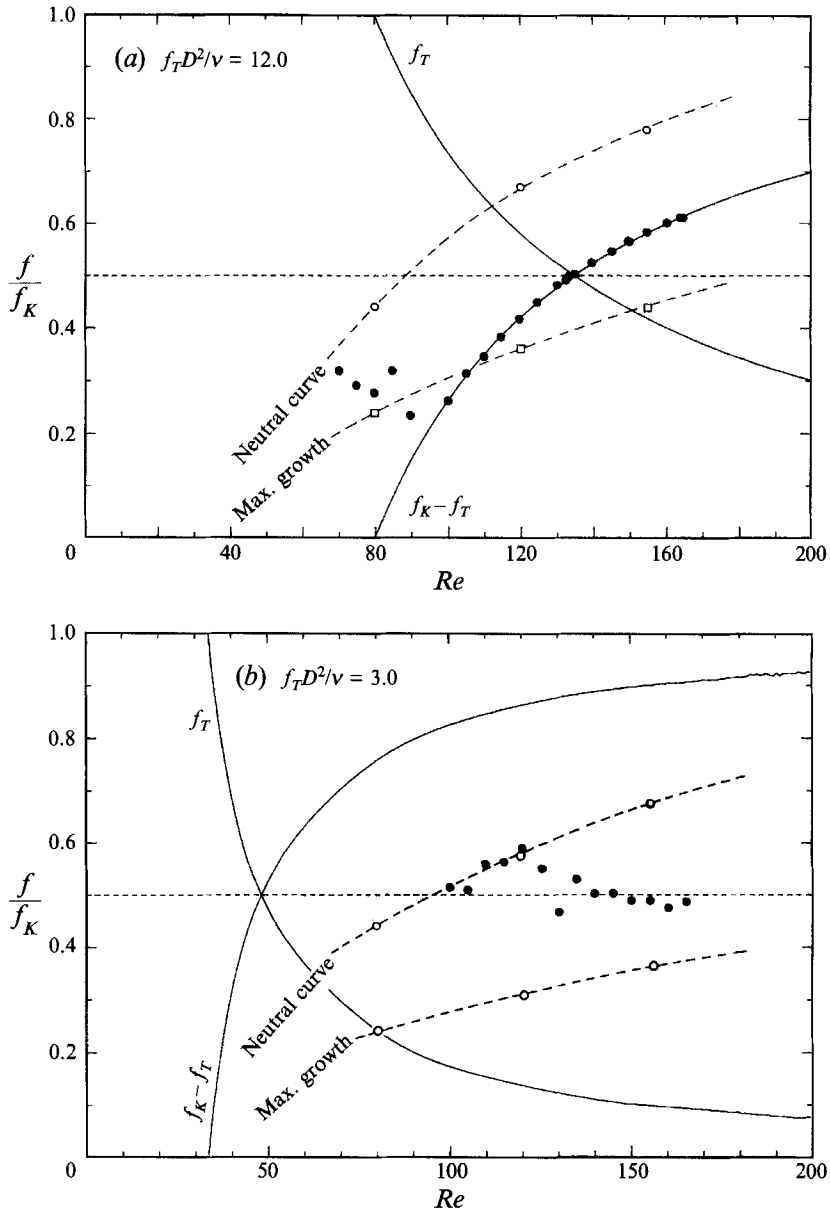

FIGURE 29. Measured and predicted normalized frequencies (f/f_K) versus Re. The experimental data are compared with a neutral stability curve and a maximum growth rate curve, based on local calculations at the far-wake distance X_{FW}. (*a*) Wake for large cylinder, (*b*) wake for small cylinder.

to yield the normalized frequencies corresponding to neutral or maximum growth rate, for a range of Re, shown in figure 29. These results are also shown in table 1. The main point to be made, from figure 29, is that for the resonant wake in (*a*), the oblique waves curve falls inside the region of linear instability in the (f, Re)-plane, whereas for the non-resonant wake in (*b*), the oblique-waves curve falls well outside the region of instability. In the latter case, the two-dimensional waves curve is far below the region of strong far-wake response (except perhaps very far downstream).

Finally, given the sensitivity of the far wake to free-stream spectral peaks, one can

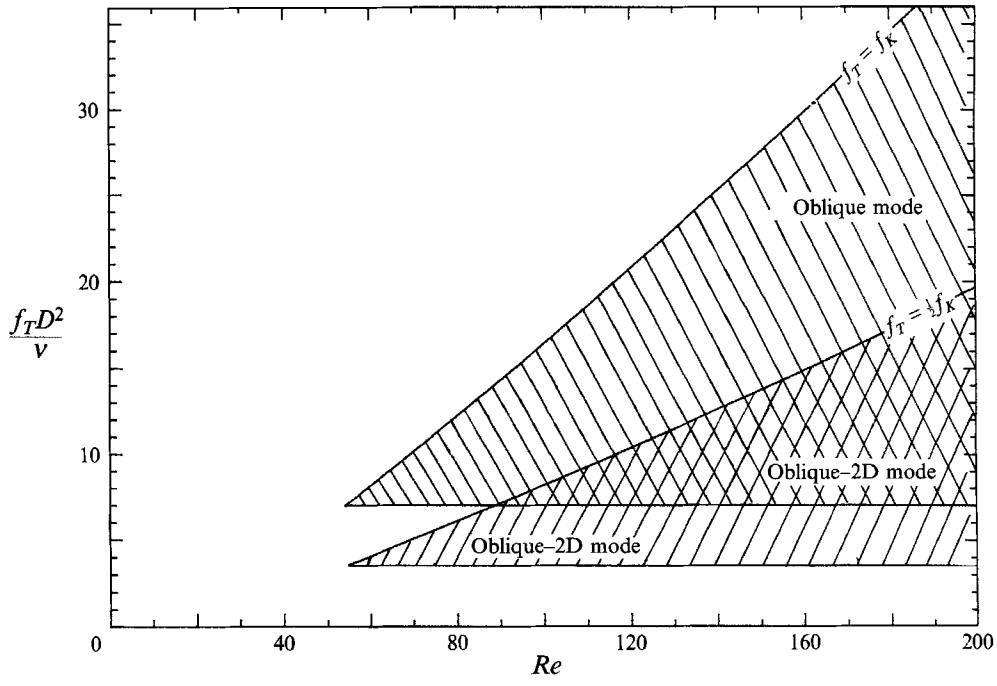

FIGURE 30. Regions for oblique wave resonance modes in the (f_T, Re)-plane.

Re	$(x/D)_{FW}$	$(W_0/U_\infty)_{FW}$	$(\delta/D)_{FW}$	$\beta_{\max}$	β_{neutral}	S_K	$(f/f_K)_{\max}$	$(f/f_K)_{\text{neutral}}$
			Resonant wake (large cylinder)					
80	250	0.236	3.21	0.74	1.36	0.1532	0.239	0.440
120	138	0.211	1.90	0.75	1.39	0.1741	0.361	0.670
155	88	0.343	1.39	0.71	1.26	0.1852	0.439	0.779
			Non-resonant wake (small cylinder)					
80	250	0.236	3.21	0.74	1.36	0.1532	0.239	0.440
120	193	0.18	2.25	0.756	1.42	0.1741	0.307	0.577
155	141	0.26	1.70	0.732	1.34	0.1852	0.370	0.677

TABLE 1. Calculation of frequencies for neutral stability and maximum growth rate

plot a map of oblique wave resonance in the (f_T, Re) plane, as shown in figure 30. The shaded areas denote resonance of different modes, as described in §7, whereas the unshaded areas indicate no resonance. The lines $f_T = f_K$ and $f_T = \frac{1}{2}f_K$ are the upper limits for the resonances, while the lower limits are dictated by when the oblique resonance curve falls above the neutral stability curve in figure 29(*a*). In essence, this map indicates where one may expect to observe different modes of resonance in different facilities or environments, depending on the value of any free-stream spectral peaks f_T.

10. Source of free-stream tunnel noise at f_T

It would seem difficult, without special precautions, to obtain a free-stream spectrum devoid of any very small spectral peaks whatsoever. In our own arrangement, it was felt important to investigate the source of the spectral peak at $f_T = 159$ Hz, and we set

up a small microphone facing upstream in the test section. By tapping on different parts of the wind tunnel, we attempted to isolate the source of the 159 Hz, and concluded that it did not originate from the wind tunnel itself. However, this does not exclude an amplification of some external frequency by the acoustic response of the test section itself. By simply removing the microphone from the test section and moving it around the laboratory, the source was ultimately discovered as a surprisingly small noise emanating from a 'muffin' fan cooling some auxiliary electronics, about 3 m away from the test section. (The actual audible noise can be imagined to be comparable with the sound of a modern reasonably quiet overhead projector.) An amplification by the test section itself gave a spectral peak for the velocity fluctuations just sufficient to cause resonance in the receptive far wake. (A rough calculation of organ pipe frequency for the test section gives 139 Hz assuming one end open, or 279 Hz assuming both ends open, indicating an acoustic receptivity of the test section to frequencies of this order.) It seems that the acoustic disturbances cause an oscillation of the fluid relative to the body, causing very small two-dimensional waves to 'ride' on the initial Kármán vortex wake, and then to become a trigger for far-wake response. The fact that two-dimensional waves are generated in far wakes may, perhaps in most cases, be attributed to acoustic forcing at the body rather than to the natural selection from broad-spectrum disturbances in the far wake. It may also be concluded that far-wake studies are highly sensitive to sources of noise within a laboratory which may include, for example, people talking and background music.

11. Discussion and interpretation of previous results

11.1. *Principal mechanism for the generation of a secondary vortex street*

The present work demonstrates that the far wake has an extreme sensitivity to the free-stream spectrum, in agreement with the studies by Cimbala & Krein (1990) and Desruelle (1983). This would perhaps suggest of itself that the primary cause of secondary street growth comes from the hydrodynamic instability of the far wake, rather than vortex pairing, as discussed in the Introduction. In this section, we shall further discuss the evidence to support one or the other hypothesis for far-wake growth.

In figure 31, we have assembled previous measurements of the far-wake normalized wavelength (λ_{FW}/λ_K) versus Re. In this plot, in some cases, the wavelength ratio has been inferred from frequency measurements, assuming phase-locking of the wake structures. Aside from the obvious scatter amongst investigators, there is generally a similar trend from the different studies, and it is one which would suggest a combination-frequency type of resonance, as found in the present work. Assuming phase-locking of the far-wake structure, one may write

$$\frac{\lambda_{FW}}{\lambda_K} = \frac{f_K}{f_{FW}} = \frac{f_K}{f_K - f_T} = \frac{1}{1 - f_T/f_K}, \tag{19}$$

so that as Re reduces, f_T/f_K will increase, and λ_{FW}/λ_K will increase. The trend of the previous studies is thus consistent with the existence of a far-wake response to free-stream spectral peaks. In order to further confirm the above suggestions, we have taken a set of data for the far-wake frequency from Matsui & Okude (1981) for their 1.2 mm cylinder, and have replotted it as normalized frequency (f/f_K) versus Re, in figure 32. There is a remarkable agreement of their data with a curve representing a combination

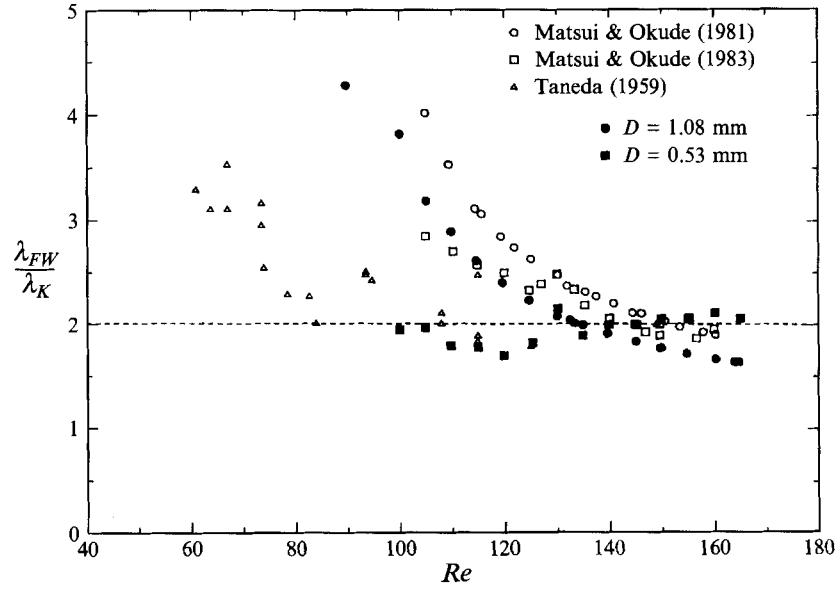

FIGURE 31. Scatter in measurements of normalized far-wake wavelength (λ_{FW}/λ_K) versus Re.

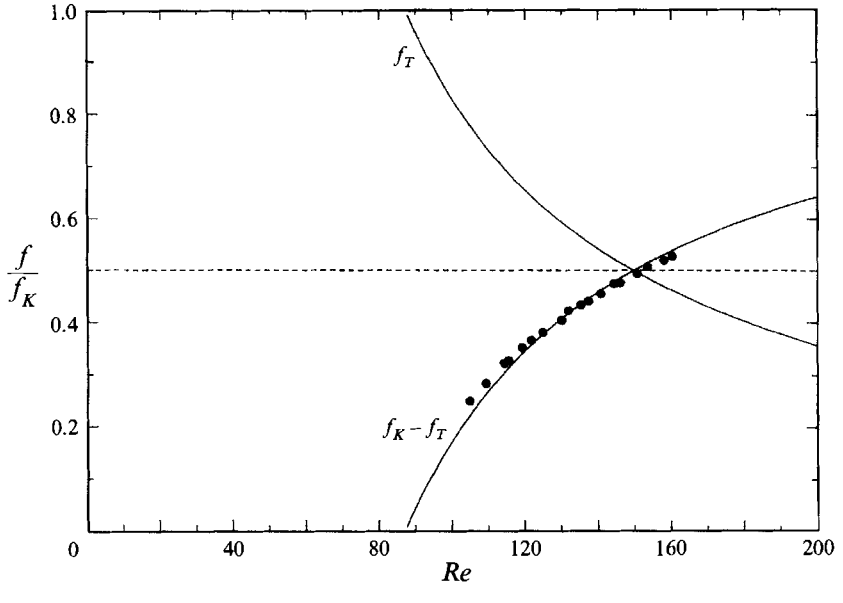

FIGURE 32. Replot of Matsui & Okude (1981) data (●) as normalized frequency (f/f_K) versus Re. Data for their 1.2 mm cylinder are used. The plot demonstrates that they had a tunnel interference frequency of $f_T D^2/\nu = 13.8$.

frequency response ($f_K - f_T$), for the particular case of ($f_T D^2/\nu$) = 13.8. This seems to be convincing evidence to show that their far wake is responding to a spectral peak of constant frequency in the free stream, and has no particular tendency for the $\frac{1}{2}$ subharmonic, despite the fact that vortex pairing was the main conclusion from their study. In the work of Matsui & Okude, vortex pairing was observed in visualizations,

although in this case they chose $Re = 140$, which corresponds to $f_{FW}/f_K = 0.45$. This is close to the $\frac{1}{2}$ subharmonic, and would yield pairing over a proportion of the cycles. It appears that pairing in their case is an incidental phenomenon, and the principal mechanism for secondary street growth is the hydrodynamic instability of the far wake responding to the free-stream spectrum, as in the present work.

The present wake response for the non-resonant case (the small cylinder wake) yields values of frequency reasonably close to the $\frac{1}{2}$ subharmonic, from which it would be tempting to suggest again that vortex pairing is the driving mechanism for far-wake growth. However, the stability calculations of Cimbala *et al.* would also suggest far-wake frequencies in the vicinity of the $\frac{1}{2}$ subharmonic. The most convincing point is perhaps the fact that the upstream shedding is oblique whereas the downstream waves are initially two-dimensional, so that vortex pairing cannot possibly be the principal cause of far-wake growth.

11.2. *'Connection' between near wake and far wake*

It was suggested in the work of Cimbala *et al.* that the far-wake three-dimensional pattern may reflect the presence of a secondary parametric instability of the subharmonic type acting on the far-wake initially two-dimensional structures. Consistent with this possibility is their suggestion that the far-wake structure does not depend directly on the scale or frequency of Kármán vortices shed from the cylinder. More recently, a connection of spanwise lengthscale was demonstrated in Williamson & Prasad (1993*a*) and in Hammache & Gharib (1992). However, it is not possible to have a connection in scale without nonlinear wave interactions. As shown in this work, there is therefore a connection between the near- and far-wake frequencies, as well as the lengthscales.

11.3. *Wave interactions for parallel shedding*

When the wake vortices shed parallel to the cylinder, there appears to be a combination-frequency resonance in the far wake, similar to that for oblique shedding. This similarity may be demonstrated from typical measurements of velocity fluctuations as a function of downstream distance, from the spectra, and from many other measurements like those made for this study, including the differences in phenomena between the small- and large-cylinder wakes.

11.4. *Oblique wave resonance in other shear flows*

The problem of the far-wake development of an 'unseparated' wake from a splitter plate or from a symmetric airfoil has a close similarity with the present study. Lasheras & Meiburg (1990) studied the three-dimensional vorticity modes in the wake of a splitter plate, in a combined experimental–numerical investigation. By computing the flow with input disturbances comprising a two-dimensional wave and pairs of oblique subharmonic waves, they found striking similarities between their computed streakline three-dimensional pattern and the flow visualization of Cimbala *et al.*

The present oblique wave resonance is similar to a combination-frequency resonance that is discussed in Raetz (1959) and in Stuart (1962). More recent experiments by Corke (1990) and analytical investigations by Mankbadi (1993) are also concerned with (combination-frequency) resonance between two- and three-dimensional waves in boundary-layer flows. These studies are related to the original 'triad' resonance introduced by Craik (1971), and which required the two- and three-dimensional subharmonic waves to be eigensolutions of the Orr–Sommerfeld equations. Corke (1990) investigated the effect of detuning the oblique pairs of waves away from the $\frac{1}{2}$-

subharmonic, and found that a family of combination frequencies appeared in an increasingly complex fashion as the flow developed. In the work of Mankbadi (1993), a critical-layer asymptotic analysis is given for the fully coupled interaction of frequency-detuned modes in a boundary layer. The analysis indicates that the interaction between a two-dimensional plane mode at frequency ω_1, and a pair of symmetrical oblique waves at near-subharmonic frequency $(\omega_1/2)(1+\Delta)$ amplifies another pair of symmetrical modes at what he terms a 'mirror frequency' $(\omega_1/2)(1-\Delta)$. The latter result is similar to the present work. If we denote the input oblique frequency as $\omega_2 = (\omega_1/2)(1+\Delta)$ and the mirror frequency as $\omega_3 = (\omega_1/2)(1-\Delta)$, then we find $\omega_3 = \omega_1 - \omega_2$. This third wave is thus a combination-frequency response as we find here for the wake resonance. In both cases, the combination frequency corresponds to oblique waves.

There are clearly similarities between the present oblique wave resonance in the wake and the resonance studies for detuned subharmonics of Corke (1990) and Mankbadi (1993) for the boundary layer. However, there are distinct differences, as follows. In these other investigations, the fundamental is a parallel two-dimensional wave, and the near-subharmonic (larger wavelength) disturbance is a pair of symmetric oblique waves. In our case, the fundamental is instead a single oblique wave, while the larger-wavelength disturbance is a parallel wave.

12. Conclusions

This investigation demonstrates that the far wake has an extreme sensitivity to free-stream disturbances, and it is these disturbances that not only lead to a large scatter in previous wake measurements, but also are responsible for the three-dimensional regular patterns that may be visualized in the far wake. This sensitivity to disturbances makes it difficult to properly define a 'natural' wake, since its structure is exquisitely dependent on the environment in which it is studied. In analogy with the mixing layer, the 'natural' far wake is by nature an excited flow.

Under certain conditions, the far wake exhibits a 'honeycomb'-like three-dimensional pattern, which in our flow is caused by an interaction of oblique shedding waves, generated upstream at the body, and larger-scale parallel (two-dimensional) waves which evolve in the far wake. The symmetry and spanwise wavelength of Cimbala *et al.*'s (1988) three-dimensional pattern are precisely consistent with such wave interactions. With such interactions, the spanwise wavelength of the honeycomb pattern is equal to the spanwise wavelength of the oblique shedding waves, which is consistent with the recent measurements of Hammache & Gharib (1992). In the presence of parallel shedding at the body, the lack of a honeycomb pattern shows that such a three-dimensional pattern is clearly dependent on the upstream oblique vortex shedding.

It has been suggested previously that the far-wake structure does not depend directly on the scale or frequency of the Kármán vortices shed from the cylinder. Our work demonstrates that *not only the scale but also the near-wake frequency* (f_K) *can directly influence the far wake*. Surprisingly, the characteristic that forges this 'connection' between the near and far wake is the sensitivity to free-stream disturbances. Even for a very small spectral peak (f_T) in the free stream, it appears that the far wake is receptive to a combination-frequency response given by $f_{FW} = (f_K - f_T)$. The large scatter in (f_{FW}/f_K) amongst previous studies is principally caused by the broad response of the far wake to a range of free-stream spectral peaks (f_T), causing a significant variation in $(f_{FW}/f_K) = 1-(f_T/f_K)$ among different investigators.

The combination-frequency response corresponds physically to an 'oblique wave resonance', as follows. The body generates oblique shedding vortices (f_K), which decay exponentially as they travel downstream. A very small spectral peak in the free stream (f_T) is sufficient to trigger the growth of two-dimensional waves in the far wake. A quadratic nonlinear interaction between these two waves induces the rapid growth of the oblique resonance waves, at a frequency ($f_K - f_T$). Geometrically, the resonance waves correspond simply to lines that pass through the nodes formed by the intersection of the oblique shedding waves and the two-dimensional waves. One might argue that this phenomenon is an artifact of the smoke visualization technique, although measurements of velocity fluctuation for the oblique waves can be an order of magnitude larger than those for the two-dimensional waves. The oblique resonance is confirmed by placing the smoke wire at different locations downstream, as well as traversing the wire across the wake.

It is found that there exist two modes of oblique wave resonance. In the Oblique–Two dimensional mode for $(f_T/f_K) < \frac{1}{2}$, there is a significant region of oblique wave resonance followed, further downstream, by a comparable amplification of two-dimensional waves in a 'honeycomb'-like three-dimensional pattern. In the Oblique mode for $(f_T/f_K) > \frac{1}{2}$, there is a resonance of oblique waves with no comparable appearance of two-dimensional waves further downstream.

Further experiments demonstrate that, in the absence of free-stream spectral peaks in the vicinity of the Kármán shedding frequency or its subharmonic, the far wake will not resonate at a specific frequency, but will exhibit a broad frequency response at an energy level between 100–10000 times less than for a resonant wake. In this case, we observe no clear structure in the far wake. This further suggests that any regular far-wake three-dimensional pattern that may be observed in different facilities would be caused by some interaction of oblique shedding waves and free-stream-induced two-dimensional waves.

Comparison of measured frequencies with those predicted by linear stability analysis (from Cimbala *et al.*) indicates that the prominent frequencies in the far wake lie between the predicted and neutrally stable frequencies. In the (f, Re)-plane, it appears that it is necessary for the oblique-waves curve to lie within the region of linear instability defined by the neutral stability curve for resonance to occur in the far wake.

The fact that the far-wake waves have a different angle to the primary waves indicates that vortex pairing cannot be the principal mechanism for secondary street development, when there is oblique shedding. It is further shown that the data of Matsui & Okude demonstrate clearly a combination-frequency resonance in the far wake, despite the fact that they interpreted their data in terms of a vortex pairing phenomenon. Indeed, it is possible to predict the frequency causing the resonance in their facility.

The clear visualizations, in the present work, of this type of oblique resonance wave would appear to represent the first observations of such waves in a shear flow. There are basic differences between this resonance and the parametric subharmonic resonance normally induced in other shear flows, for example the channel flow, the boundary layer or the wake from an airfoil. In these other investigations, the fundamental is a two-dimensional wave, and the subharmonic secondary disturbance is a pair of symmetric oblique waves. In our case, the fundamental is instead a single oblique wave, while the larger-wavelength disturbance is a single two-dimensional wave.

The authors would like to thank Kristen Gledhill at Cornell for her enthusiastic help at the very inception of this research, and also Gregory D. Miller for invaluable

assistance with visualization and microphone measurements. Thanks are due for the hearty encouragement received from Professors Sidney Leibovich and Philip Holmes at Cornell. The authors thank also Chantal Champagne, PhD, for indispensable assistance during paper preparation. This work was supported at Cornell by an ONR Contract No. N00014-90-J-1686, as part of the ONR 'Bluff body Wake Vortex Dynamics and Instabilities' Accelerated Research Initiative.

REFERENCES

BROWN, G. L. & ROSHKO, A. 1974 On density effects and large structure in turbulent mixing layers. *J. Fluid Mech.* **64**, 775.

CIMBALA, J. M. 1984 Large structure in the far wakes of two-dimensional bluff bodies. PhD thesis, Graduate Aeronautical Laboratories, California Institute of Technology.

CIMBALA, J. M. & KREIN, A. 1990 Effect of freestream conditions on the far wake of a cylinder. *AIAA J.* **28**, 1369.

CIMBALA, J. M., NAGIB, H. M. & ROSHKO, A. 1981 Wake instability leading to new large scale structures downstream of bluff bodies. *Bull. Am. Phys. Soc.* **26**, 1256.

CIMBALA, J. M., NAGIB, H. M. & ROSHKO, A. 1988 Large structure in the far wakes of two-dimensional bluff bodies. *J. Fluid Mech.* **190**, 265.

COLES, D. 1985 The uses of coherent structure. *AIAA Dryden lecture.*

CORKE, T. 1990 Effect of controlled resonant interactions and mode detuning on turbulent transition in boundary layers. In *IUTAM Symp. on Laminar–Turbulent Transition* (ed. D. Arnal & R. Michel). Springer.

CORKE, T. 1993 Effect of mode detuning on far wake development. *J. Fluid Mech.* (to be submitted).

CORKE, T., KOGA, D., DRUBKA, R. & NAGIB, H. 1977 A new technique for introducing controlled sheets of streaklines in wind tunnels. *IEEE Publication* 77-CH 1251-8 AES.

CORKE, T., KRULL, J. D. & GHASSEMI, M. 1992 Three-dimensional mode resonance in far wakes. *J. Fluid Mech.* **239**, 99.

CORKE, T. & MANGANO, R. A. 1989 Resonant growth of three-dimensional modes in transitioning Blasius boundary layers. *J. Fluid Mech.* **209**, 93.

CRAIK, A. D. D. 1971 Nonlinear resonant instability in boundary layers. *J. Fluid Mech.* **50**, 393.

CRAIK, A. D. D. 1985 *Wave Interactions and Fluid Flows.* Cambridge University Press.

DESRUELLE, D. 1983 Beyond the Karman vortex street. M.S. thesis, Illinois Institute of Technology.

EISENLOHR, H. & ECKELMANN, H. 1989 Vortex splitting and its consequences in the vortex street wake of cylinders at low Reynolds number. *Phys. Fluids* A **1**, 189.

GERRARD, J. H. 1978 The wakes of cylindrical bluff bodies at low Reynolds number. *Phil. Trans. R. Soc. Lond.* A **288**, 351.

HAMA, F. R. 1957 Three-dimensional vortex pattern behind a circular cylinder. *J. Aeronaut. Sci.* **24**, 156.

HAMMACHE, M. 1991 APS Meeting. *Bull. Am. Phys. Soc.* **26**, 1256.

HAMMACHE, M. & GHARIB, M. 1989 A novel method to promote parallel shedding in the wake of circular cylinders. *Phys. Fluids* A **1**, 1611.

HAMMACHE, M. & GHARIB, M. 1991 An experimental study of the parallel and oblique vortex shedding from circular cylinders. *J. Fluid Mech.* **232**, 567.

HAMMACHE, M. & GHARIB, M. 1992 On the evolution of three-dimensionalities in laminar bluff body wakes. In *Proc. IUTAM Conf. on Bluff Body Wake Instabilities* (ed. H. Eckelmann & J. M. R. Graham). Springer (to appear).

HERBERT, T. 1988 Secondary instability of boundary layers. *Ann. Rev. Fluid Mech.* **20**, 487.

HO, C.-M. & HUERRE, P. 1984 Perturbed free shear layers. *Ann. Rev. Fluid Mech.* **16**, 365.

KOENIG, M., EISENLOHR, H., ECKELMANN, H. 1990 The fine structure in the *S–Re* relationship of the laminar wake of a circular cylinder. *Phys. Fluids* A **2**, 1607.

LAMB, H. 1932 *Hydrodynamics.* Cambridge University Press.

LASHERAS, J. C. & MEIBURG, E. 1990 Three-dimensional vorticity modes in the wake of a flat plate. *Phys. Fluids* A **2**, 371.

MANKBADI, R. R. 1993 Effect of mode detuning on laminar-turbulent transition in boundary layers. *AIAA Aerospace Sci Conf, Reno, Nevada*, Paper 93-0347.

MATSUI, T. & OKUDE, M. 1981 Vortex pairing in a Karman vortex street. In *Proc. Seventh Biennial Symp. on Turbulence, Rolla, Missouri.*

MATSUI, T. & OKUDE, M. 1983 Formation of the secondary vortex street in the wake of a circular cylinder. In *Structure of Complex Turbulent Shear Flow, IUTAM Symp., Marseille, 1982.* Springer.

MEIBURG, E. 1987 On the role of subharmonic perturbations in the far wake. *J. Fluid Mech.* **177**, 83.

MEIBURG, E. & LASHERAS, J. C. 1988 Experimental and numerical investigation of the three-dimensional transition in plane wakes. *J. Fluid Mech.* **190**, 1.

PIERREHUMBERT, R. & WIDNALL, S. 1982 The two- and three-dimensional instabilities of a spatially periodic shear layer. *J. Fluid Mech.* **114**, 59.

RAETZ, R. E. 1959 A new cause of transition in fluid flows. *Northrop Rep.* NOR-59-383 (BLC-121).

ROSHKO, A. 1954 On the development of turbulent wakes from vortex streets. *NACA Rep.* 1191.

STAFFMAN, P. G. & SCHATZMAN, J. C. 1982 Stability of a vortex street of finite vortices. *J. Fluid Mech.* **117**, 171.

SQUIRE, H. B. 1933 On the stability for three-dimensional disturbances of viscous fluid flow between parallel walls. *Proc. R. Soc. Lond.* A **142**, 621.

STUART, J. T. 1962 Nonlinear effects in hydrodynamic stability. In *Proc. Tenth IUTAM Cong. of Applied Mech.* (ed. F. Rolla & W. T. Koiter), pp. 91–97. Elsevier.

TANEDA, S. 1959 Downstream development of wakes behind cylinders. *J. Phys. Soc. Japan* **14**, 843.

WILLIAMSON, C. H. K. 1988*a* Defining a universal and continuous. Strouhal–Reynolds number relationship for the laminar vortex shedding of a circular cylinder. *Phys. Fluids* **31**, 2742.

WILLIAMSON, C. H. K. 1988*b* The existence of two stages in the transition to three-dimensionality of a cylinder wake. *Phys. Fluids* **31**, 3165.

WILLIAMSON, C. H. K. 1989*a* Oblique and parallel modes of vortex shedding in the wake of a circular cylinder at low Reynolds numbers. *J. Fluid Mech.* **206**, 579.

WILLIAMSON, C. H. K. 1989*b* Generation of periodic vortex dislocations due to a point disturbance in a planar wake. In the *Gallery of Fluid Motion, Phys. Fluids* A **1**, 1444.

WILLIAMSON, C. H. K. 1991 Three-dimensional aspects and transition in the wake of a cylinder. In *Turbulent Shear Flows* (ed. F. Durst & J. Launder), pp. 173–194. Springer.

WILLIAMSON, C. H. K. 1992*a* The natural and forced formation of a spot-like 'vortex dislocations' in the transition of a wake. *J. Fluid Mech.* **243**, 393.

WILLIAMSON, C. H. K. 1992*b* Wave interactions in the far wake. In *Proc. IUTAM Conf. on Bluff Body Wake Instabilities* (ed. H. Eckelmann & J. M. R. Graham). Springer (to appear).

WILLIAMSON, C. H. K. & PRASAD, A. 1993*a* Oblique wave interactions in the far wake. *Phys. Fluids* A **5**, 1854.

WILLIAMSON, C. H. K. & PRASAD, A. 1993*b* Acoustic forcing of oblique wave resonance in the far wake. *J. Fluid Mech.* **256**, 315.

WINANT, C. D. & BROWNAND, F. K. 1974 Vortex pairing: the mechanism of turbulent mixing layer growth at moderate Reynolds number. *J. Fluid Mech.* **63**, 237.